Am J Nucl Med Mol Imaging 2013;3(3):194-216
www.ajnmmi.us /ISSN:2160-8407/ajnmmi1302002

Review Article

PET radiopharmaceuticals for probing enzymes in the brain

Jason P Holland[1], Paul Cumming[2], Neil Vasdev[1]

[1]*Division of Nuclear Medicine and Molecular Imaging, Massachusetts General Hospital, and Department of Radiology, Harvard Medical School, 55 Fruit St., White 427, Boston, MA 02114, USA;* [2]*Department of Nuclear Medicine, Universitätsklinikum Erlangen, Ulmenweg 18, Erlangen, Germany, 91054*

Received January 6, 2013; Accepted March 7, 2013; Epub April 9, 2013; Published April 15, 2013

Abstract: Biologically important processes in normal brain function and brain disease involve the action of various protein-based receptors, ion channels, transporters and enzymes. The ability to interrogate the location, abundance and activity of these entities *in vivo* using non-invasive molecular imaging can provide unprecedented information about the spatio-temporal dynamics of brain function. Indeed, positron emission tomography (PET) imaging is transforming our understanding of the central nervous system and brain disease. Great emphasis has historically been placed on developing radioligands for the non-invasive detection of neuroreceptors. In contrast, relatively few enzymes have been amenable to examination by PET imaging procedures based upon trapping or accumulation of enzymatic products, because only a subset of enzymes have sufficient catalytic rate to produce measureable accumulation within the practical time-limit of PET recordings. However, high affinity inhibitors are now serving as tracers for enzymes, particularly for measuring the abundance of enzymes mediating intracellular signal transduction in the brain, which offer a rich diversity of potential targets for drug discovery. The purpose of this review is to summarize well-known radiotracers for brain enzymes, and draw attention to recent developments in PET radiotracers for imaging signal transduction pathways in the brain. The review is organized by target class and focuses on structural chemistry of the best-established radiotracers identified in each class.

Keywords: Positron emission tomography, monoamines, second messengers, kinase inhibitors, esterases

Introduction

Enzymatic catalysis entails the binding of one or more substrates to specific domains of the enzyme, followed by a thermodynamically favored chemical reaction, sometimes driven by the expenditure of a molecule of ATP or other co-substrates. The reaction is followed by conformational changes in the protein leading to release of the enzymatic products. The assay of enzyme activity *in vitro* typically consists of measuring the rate of product formation or substrate consumption *versus* time, under standard conditions and at a specified temperature (usually 37°C). Monitoring the reaction rate can entail a spectroscopic measure that changes during the reaction, such as optical rotation, UV/visible electronic absorption, or fluorescence emission. In some cases it may be necessary to separate chemically the product from the reaction mixture using chromatography or other extraction procedures, or by trapping of a gaseous product, as in classical assays of decarboxylase enzymes where the rate of radioactive CO_2 production is measured *in vitro*. However, in the crucible of the living brain, such procedures cannot readily be employed.

How can we chart the biological distribution of an enzyme, and measure its expression level and activity *in vivo*? Arguably, the most promising answer to this fundamental challenge of neuroscience lies in the development of small molecules labeled with positron-emitting radionuclides such ^{11}C and ^{18}F, that can be used for non-invasive dynamic imaging by positron emission tomography (PET). Whereas the biochemist can separate an enzymatic product, PET procedures for measuring enzyme activity rely upon the retention of an enzymatic product in the medium of the brain, and the *mathematical* separation of substrate-product concentrations

as a function of time. There is a relative paucity of brain enzymatic processes meeting the dual criterion that the substrate must be diffusible across the blood brain barrier while the product must be retained in sufficient quantity to produce a measurable signal. More often, enzyme abundance, as distinct from enzyme activity, is measured using positron-emitting inhibitors, which bind to the target molecule in the manner of a receptor-ligand interaction, but without being substrates for the enzymatic process under consideration. This review presents a synopsis of the state of development of PET procedures for assaying enzymes in the living brain. We illustrate first those radiotracers that can be used to monitor protein synthesis, energy metabolism, and cell proliferation, then radiotracers for neurotransmitter synthesis and metabolism, and finally a series of novel radiotracers targeting other metabolic processes in brain, emphasizing the new chemical developments for imaging intracellular systems. This review is derived from earlier book chapters which focused on imaging and kinetics [1, 2].

Hexokinase and the cerebral metabolism of glucose

Of the thousands of reports on [^{18}F]-fluorodeoxyglucose ([^{18}F]-FDG), there is a great preponderance of clinical oncology PET studies, although the original application of [^{18}F]-FDG PET was to study cerebral glucose metabolism [3]. Most tumors take up [^{18}F]-FDG faster than do most healthy tissues, which explains the interest of [^{18}F]-FDG PET for clinical oncology. Uniquely, the brain is normally entirely dependent on glucose for energy metabolism, and the brain has a voracious appetite for energy derived from the anaerobic and aerobic metabolism of glucose. [^{18}F]-FDG is scarcely metabolized in circulation, and enters the brain by a facilitated diffusion process mediated by glucose transporter-1 (GLUT-1) in the blood-brain barrier [4]. Uptake in neuronal cells is predominantly mediated by glucose transporter-3 (GLUT-3) [4]. By the conventions of tracer kinetics, the initial clearance of [^{18}F]-FDG into brain is termed K_1, which has units of cerebral blood flow (ml g^{-1} min^{-1}). Free [^{18}F]-FDG in brain can diffuse back to circulation, but inside living cells, [^{18}F]-FDG is phosphorylated by hexokinase, the first and rate-limiting enzyme in the glycolytic pathway. The activity of hexokinase relative to [^{18}F]-FDG, thus determines the cerebral metabolic rate for glucose, which is normally the only source of carbon for brain energy metabolism. The hexokinase product [^{18}F]-FDG-phosphate is not a substrate for subsequent enzyme-mediated reactions, but is retained in living cells due to its high charge, and accumulates as a function of the hexokinase activity, or may be slowly dephosphorylated. Knowing the concentration of [^{18}F]-FDG in serial samples of arterial blood, data from a dynamic PET recording can be calculated as the net radiotracer influx to brain, which is an index of the cerebral metabolic rate for glucose.

The utility of [^{18}F]-FDG PET for neuro-oncology is limited by the very high physiological uptake of glucose by normal brain tissue, such that tumor-to-background ratios are low. [^{18}F]-FDG PET may be more useful for neurodegenerative diseases, in which radiotracer uptake is reduced due to impaired metabolism. The sensitivity of [^{18}F]-FDG PET for diagnosis of Alzheimer's disease is the subject of a recent review [5]. In one landmark study, [^{18}F]-FDG scans were obtained in a series of cognitively normal elderly patients, with follow-up over a period of more than 10 years [6]. Some subjects proceeded to develop Alzheimer's-type dementia, which was ultimately confirmed by post-mortem analysis. Results showed reductions in [^{18}F]-FDG trapping years in advance of the emergence of clinical symptoms, highlighting the potential of [^{18}F]-FDG PET for monitoring disease-modifying intervention studies. Further brain diseases amenable to diagnosis [^{18}F]-FDG PET include medically refractory focal epilepsies, as epileptogenic foci exhibit decreased glucose metabolism, which helps in their localization prior to resection [7].

Amino acid transport

In theory, any of the 21 natural amino acids could serve as a tracer for protein synthesis or transport. One of the first molecular imaging agents for PET was the amino acid *L*-[^{11}C]-methionine, obtained in the laboratory by S-[^{11}C]methylation (**Figure 1**) [8]. This radiotracer enters several metabolic pathways such as protein synthesis and conversion to *S*-adenosylmethionine, which is the main biological methyl group donor and precursor of cysteine and derivatives. Serial PET recordings

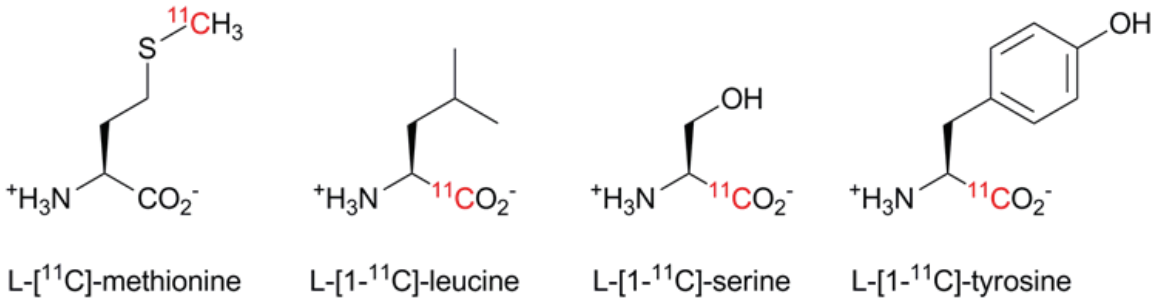

Figure 1. Structures of four of the most prominent ^{11}C-radiolabeled amino acids.

after intravenous injection of *L*-[^{11}C]-methionine reveal a substantial uptake of radioactivity into pancreas, brain, and other organs with high rates of protein synthesis. Amino acids are not freely diffusible across the blood-brain barrier, but are exchanged by facilitated diffusion carriers, which is mediated in the case of *L*-methionine by the leucine-favoring (L1-type) amino acid transporter [9]. Upon entering brain cells, *L*-[^{11}C]-methionine binds to transfer-RNA and is then incorporated into newly-synthesized proteins. This trapping is irreversible relative to the 20 minute half-life of the radionuclide. Due to the rapid protein synthesis which is inherent to many tumors, *L*-[^{11}C]-methionine PET has been extensively used in neuro-oncology. In an early clinical PET study, the uptake of *L*-[^{11}C]-methionine correlated with histological grade of glial tumors, and declined following radiotherapy [10]. The use and limitations of *L*-[^{11}C]-methionine PET in the clinical monitoring of gliomas has been reviewed [11].

The specificity of a given amino acid radiotracer for protein synthesis is influenced by the occurrence of alternate metabolic pathways. In particular, cerebral trapping of *L*-[^{11}C]-methionine, and likewise *L*-[^{11}C]-leucine (**Figure 1**), cannot be exclusively attributed to protein synthesis. Radiochromatograms of plasma extracts from human subjects reveal at least three metabolites of *L*-[^{11}C]-methionine, including *L*-[^{11}C]-serine (**Figure 1**), which should be considered a second input to brain protein synthesis [12]. Whereas *L*-[^{11}C]-methionine also has transmethylation products derived from *S*-adenosyl-*L*-methionine, carboxylic acid labeling is metabolically more restricted, giving rise only to [^{11}C]-CO_2, which is rapidly eliminated from brain [13]. The distribution of carboxymethyl-labeled *L*-[^{11}C]-tyrosine in rat tumors had more favorable specificity: some 80% of tissue radioactivity was bound to protein after one hour [14]. It is important to note that the net trapping of labeled amino acids in brain protein is inherently less than the true rate of protein synthesis, due to the generation of amino acids *in situ* through proteolysis; thus, the tracer may not attain equilibrium with the precursor pool in brain.

In one of the few non-oncological human PET imaging studies using protein synthesis radiotracers, the cerebral trapping of *L*-[^{11}C]-methionine was reduced by 20% in grey matter of patients with Alzheimer's disease, indicating a global reduction in protein synthesis [15]. In a *L*-[^{11}C]-tyrosine (**Figure 1**) study of phenylketonuria, there was an inverse relationship between plasma phenylalanine levels and radiotracer uptake in brain, indicative of substrate limitation arising from competition for blood-brain barrier transport [16]. In a *L*-[1-^{11}C]-leucine PET study of healthy volunteers, propofol anesthesia was without effect on the rate of protein synthesis in brain [17]. However, brain protein synthesis in patients with fragile X syndrome and in corresponding transgenic mice was responsive to propofol anesthesia, suggesting an abnormal relationship between synaptic signaling and protein formation [18].

Cell proliferation

The mechanisms mediating transport of nucleosides such as thymidine across the blood-brain barrier are complex and poorly understood [19]. As with protein synthesis, PET measurements of cell proliferation using labeled nucleosides do not normally account for the generation of precursors *in situ*, either by salvage pathways or *de novo* nucleotide synthesis. Despite these uncertainties, the synthesis of nucleotides, the precursors for nucleic

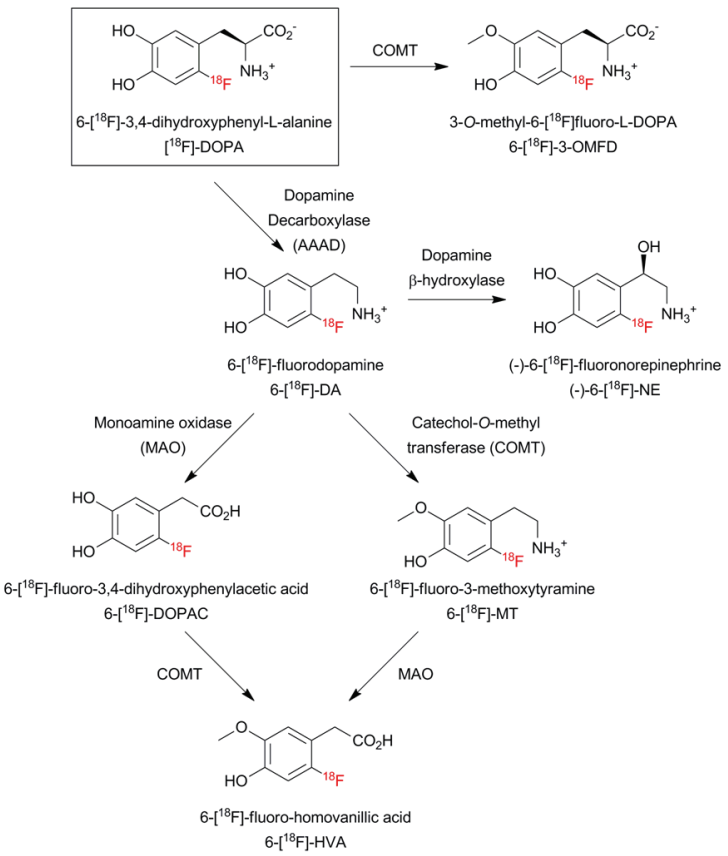

Figure 2. Structures of 6-[^{18}F]-DOPA and related metabolites. COMT = catechol *O*-methyl transferase; MAO = monoamine oxidase; Dopamine decarboxylase is also know as aromatic L-amino acid decarboxylase (AAAD).

acid synthesis, can be detected in living brain in the PET studies with the nucleoside [^{11}C]-thymidine, although this tracer undergoes rapid metabolism *in vivo*, with generation of a number of labeled metabolites [20]. A better PET proliferation tracer would have more constrained metabolism, in analogy to the case of [^{18}F]-FDG. To this end, the synthetic nucleoside 3'-deoxy-3'-[^{18}F]-fluorothymidine ([^{18}F]-FLT) was developed [21]. It is entrapped as [^{18}F]-FLT-phosphate by a specific thymidine kinase (thymidine kinase-1 or TK1) that is mainly expressed in dividing cells. Also like [^{18}F]-FDG-phosphate, [^{18}F]-FLT-phosphate does not proceed farther in the normal metabolic pathway. [^{18}F]-FLT is at least as sensitive as [^{18}F]-FDG for the detection of gliomas, and may have lesser uptake in healthy brain tissue, imparting better contrast. Compared to the radiolabeled amino acids, however, this substance may fail to visualize the better differentiated parts of gliomas, as a prerequisite to its uptake in brain is a blood brain barrier disruption. An acute reduction in tumoral [^{18}F]-FLT uptake was predictive of survival in patients treated for recurrent gliomas [22]. Net influx for [^{18}F]-FLT relative to the arterial input (*K*) sensitively revealed the proliferative zone in astrocytoma tumors, with much less background uptake in healthy tissue than was seen with the protein synthesis radiotracer [^{11}C]-methionine. Detailed kinetic analysis of dynamic [^{18}F]-FLT data could be used to evaluate the relative activity of thymidine kinase in brain tumors, and suggested the presence of a slow dephosphorylation of the radiotracer , as can also be discerned with [^{18}F]-FDG PET [23].

Neurotransmitter synthesis

Dopamine

The immediate precursor for dopamine synthesis is 3,4-dihydroxy-*L*-phenylalanine (*L*-DOPA), which is derived from tyrosine. The development of the synthetic *L*-DOPA decarboxylase substrate 6-[^{18}F]-fluoro-3,4-dihydroxyphenyl-*L*-alanine ([^{18}F]-DOPA) was an early success of molecular brain imaging (**Figure 2**) [24, 25]. [^{18}F]-DOPA in circulation crosses the blood-brain barrier by facilitated diffusion mediated by the L-type carrier of large neutral amino acids. Since [^{18}F]-DOPA influx is inhibited by competition from the other amino acid substrates [26], [^{18}F]-DOPA PET scans are best conducted in a fasting condition. [^{18}F]-DOPA is a good substrate for DOPA decarboxylase [27] in nigrostriatal dopamine fibres, which retain the product 6-[^{18}F]-fluorodopamine (6-[^{18}F]-DA) in synaptic vesicles [28]. However, the implicit model for [^{18}F]-DOPA metabolism is inherently complex, as recently reviewed [29]. [^{18}F]-DOPA is a substrate for hepatic catechol-*O*-methyltransferase (COMT) [30], such that substantial amounts of the metabolite 3-*O*-methyl-6-[^{18}F] fluoro-*L*-DOPA (6-[^{18}F]-3-OMFD; **Figure 2**) accumulate in plasma [31]. This product enters brain by the same carrier as [^{18}F]-DOPA, and

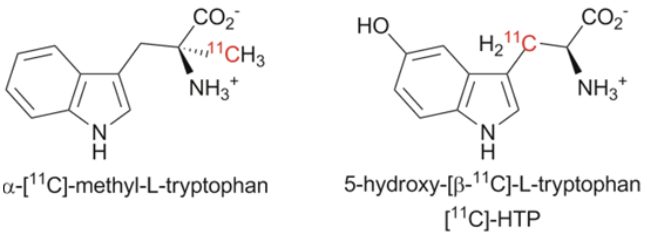

Figure 3. Structures of two ^{11}C-radiotracers based on the amino acid L-tryptophan.

soon constitutes the main component of non-specific background signal throughout the brain [32, 33]. Furthermore, 6-[^{18}F]-DA is not perfectly retained in synaptic vesicles, but is slowly decomposed by monoamine oxidase (MAO) [34] to yield the diffusible metabolites 6-[^{18}F]-DOPAC and 6-[^{18}F]-HVA; significant washout occurs during prolonged PET recordings [35]. Finally, [^{18}F]-DOPA trapping is not entirely specific for dopamine fibres, since metabolism in serotonin fibres contributes to the PET signal [36].

Despite the complexities of its metabolism, [^{18}F]-DOPA is one of the most widely used radiotracers for PET studies of brain physiology, especially for monitoring nigrostriatal degeneration of Parkinson's disease (PD) and related disorders. PET studies with [^{18}F]-DOPA have revealed subclinical nigrostriatal degeneration in kindred with hereditary Lewy body PD [37], the rate of progression of idiopathic PD [38], and the possible attenuation of that progression through treatment with a dopamine agonist [39]. [^{18}F]-DOPA PET serves for the discriminative diagnosis of PD and a number of other basal ganglia diseases [29], and has given new insight into the pathophysiology of schizophrenia; elevated dopamine synthesis capacity has been reported in striatum of untreated patients with schizophrenia [40]. An application of an extended kinetic model revealed that not only is the rate of 6-[^{18}F]-DA synthesis increased in patients with schizophrenia, but its rate of breakdown and washout is also elevated [41], a phenomenon which has been described as "poverty in the midst of plenty", due to the seemingly poor retention of 6-[^{18}F]-DA in synaptic vesicles.

Serotonin

Despite wide acceptance of a serotonin hypothesis of depression, there is little direct evidence for a serotonergic abnormality in affective disorders. Presynaptic serotonin synthesis can be probed in PET studies with the direct precursor 5-hydroxy-[^{11}C]-*L*-tryptophan (**Figure 3**) [42], with the caveat that this molecule is also a substrate for DOPA decarboxylase which is present in serotonin and dopamine fibres. Like the other large neutral amino acids, α-methyl-*L*-tryptophan is transferred reversibly across the blood-brain barrier; in serotonin terminals, it is a substrate for tryptophan hydroxylase (without any concomitant labeling of brain protein), and the product α-methyl-5-hydroxy-*L*-tryptophan yields α-methylserotonin. Although theoretically elegant, the rate of conversion of α-[^{11}C]-methyl-*L*-tryptophan (**Figure 3**) is slow, and its sensitivity for PET assays of serotonin synthesis has been questioned [43]. However, others found a good correlation between the net influx of α-[^{11}C]-methyl-*L*-tryptophan and that of the DOPA decarboxylase substrate 5-hydroxy-[^{11}C]-*L*-tryptophan [42], and a high correlation with post mortem serotonin concentrations [44].

Parametric mapping with α-[^{11}C]-methyl-*L*-tryptophan revealed focal cortical reductions in patients with major depression [45], and in suicide attempters [46]. In another depression study, stimulation of α-[^{11}C]-methyl-*L*-tryptophan influx to the prefrontal cortex by treatment with a serotonin reuptake inhibitor was augmented by co-treatment with an antagonist of autoreceptors on serotonin neurons [47], consistent with a theory predicting synergistic action of the two medications in the treatment of depression. Cortical foci of increased α-[^{11}C]-methyl-*L*-tryptophan uptake are associated with epileptogenic dysplasia in children with tuberous sclerosis [48], and can potentially guide the planning of surgical resection [49], but the physiological basis of this trapping is obscure.

Neurotransmitter catabolism

Monoamine oxidase

As noted above, MAO catalyzes the oxidative deamination of dopamine, and also other biogenic amines such as serotonin. MAO occurs in two forms with somewhat differing substrate specificities and distributions; whereas MAO-A prefers serotonin and noradrenaline and MAO-B prefers β-phenylethylamine, both

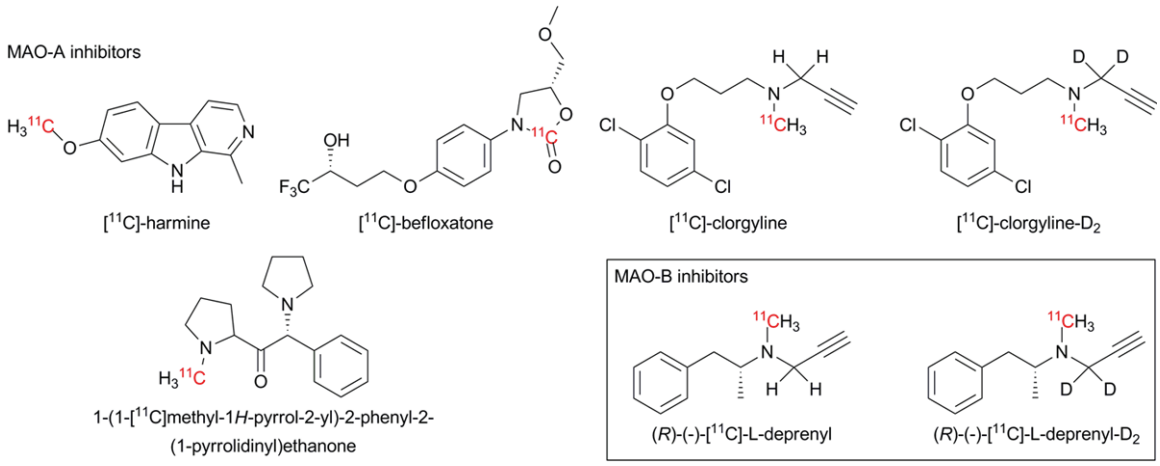

Figure 4. Structures of selected ^{11}C-radiolabeled MAO inhibitors [68, 175-178].

enzymes equally catalyze the deamination of dopamine and tryptamine [50]. As such, MAOs are important targets for molecular imaging of monoaminergic systems; in brain, MAO-A is most highly expressed in noradrenaline neurons [50], while MAO-B is most abundant in serotonin neurons and the tuberomammillary histamine neurons [51]. Many radiotracers have been developed for imaging MAO-B (see references [52] and [53] for reviews).

The first PET tracer for MAO was the MAO-B substrate [^{11}C]-MPTP, which accumulates in the striatum of rhesus monkey, apparently by the same enzymatic trapping mechanism underlying the notorious toxicity of that compound for dopamine neurons [54, 55], i.e. generation of [^{11}C]-MPP$^+$ *in situ*. More promising for human PET studies are the suicide substrates [^{11}C]-clorgyline and [^{11}C]-deprenyl (**Figure 4**) for imaging MAO-A and MAO-B, respectively [56]. Consistent with a mechanistic understanding of the rapid and irreversible binding of these suicide substrates, α-deuterated [^{11}C]-deprenyl ([^{11}C]-deprenyl-D_2) reacted with a substantial isotope effect (3.8 ± 1.1 rate enhancement for trapping of hydrogen *versus* deuterium isotopomer) [57]. In an early clinical application of [^{11}C]-deprenyl-D_2, there was increased binding within epileptic foci of the human temporal lobe, presumably reflecting MAO-B expression in reactive astrocytes [58].

[^{11}C]-Deprenyl-D_2 has been used in a competition paradigm to test the extent of occupancy of a novel drug at MAO-B sites in human brain [59]. The discovery of reduced MAO-B activity in brain and peripheral organs of smokers suggests the presence of a potent inhibitor in tobacco smoke [60]. The inhibition must be cumulative, since smoking a single cigarette was without effect on [^{11}C]-deprenyl-D_2 binding [61]. The deuterium isotope effect proved less useful for the case of [^{11}C]-clorgyline, due to the emergence of a non-MAO-A binding component in white matter [62]. Inhibition of MAO-A was revealed in brain of smokers in a PET study with [^{11}C]-clorgyline [63].

Reversibly binding MAO ligands might present advantages over the irreversible enzyme substrates discussed above. Binding of the MAO-A ligand 1-(1-[^{11}C]methyl-1*H*-pyrrol-2-yl)-2-phenyl-2-(1-pyrrolidinyl)ethanone in pig brain MAO was displaced by pre-treatment with an MAO inhibitor [64] (**Figure 4**), but this compound has not yet found clinical PET applications. The β-carboline [^{11}C]-harmine (**Figure 4**) binds reversibly to MAO-A *in vitro* with an affinity of 2 nM [65], and has been used in human PET studies for assessment of the central occupancy of MAO-A by novel inhibitors [65], and by constituents of St. John's Wort (*Hypericum perforatum*) [66]. The earlier report of MAO-A inhibition in brain of smokers was recently confirmed in a study with the reversible MAO-A ligand [^{11}C]-befloxatone [67, 68] (**Figure 4**), and cessation of smoking results in acute increases in [^{11}C]harmine binding [69]; this increase was associated with transient depression in healthy non-smokers, presumably due to enhanced metabolism of dopamine and serotonin. However, in preclinical studies, a nearly complete inhibition of both forms of MAO failed to

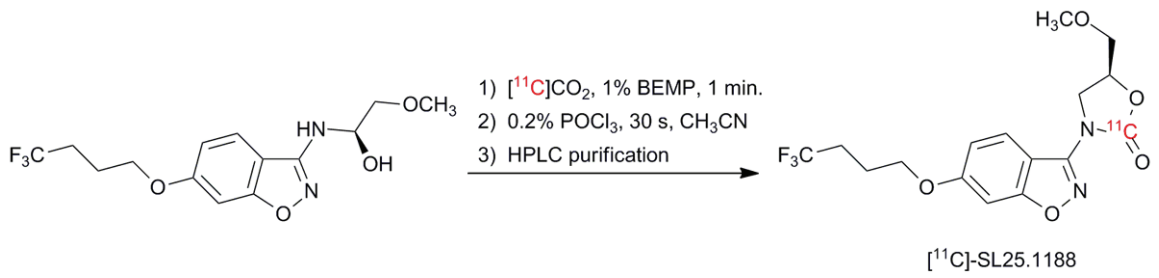

Figure 5. Synthesis of [^{11}C]-SL25.1188 using [^{11}C]-CO_2 fixation [85].

evoke any potentiation of the displacement of [^{11}C]-raclopride by amphetamine-evoked dopamine release [70, 71]. Increased [^{11}C]-harmine uptake in cerebral cortex has been described in brain of untreated, non-smoking depressed patients [72], and persistence of this increase following pharmacotherapy may predict for relapse [73], presumably due to increased neurotransmitter catabolism. Increased [^{11}C]-harmine uptake, presumably of a transient nature, is also described in women in the early postpartum period [74]. A more recent study using [^{11}C]-harmine measured the effect of changes in MAO-A substrate on MAO-A binding in regions implicated in affective and neurodegenerative disease in healthy volunteers and the findings of this work suggest an adaptive role for MAO-A in maintaining monoamine neurotransmitter homeostasis by rapidly compensating fluctuating monoamine levels [75].

While [^{11}C]-harmine has excellent properties as a reversible MAO-A ligand, a reversible ligand with selectivity for MAO-B imaging has remained elusive. The search for such a compound is motivated by a potential use in PET studies of Parkinson's disease, in which MAO-B has been implicated, based upon the MAO-B-catalyzed toxicity of MPTP for dopamine neurons. In one approach, the reversible and selective MAO-B inhibitor Ro-19-6327 was radiolabeled by replacing the chlorine with radioiodine, giving [^{123}I]-Ro-43-0463 [76] or ^{18}F for PET studies; both radiotracers were evaluated in human subjects [77]. While [^{123}I]-Ro-43-0463 had good properties for SPECT imaging, the ^{18}F-analog had limited brain uptake. It is noteworthy that ^{18}F-radiolabeled analogues of deprenyl [78, 79] and rasagyline [80] have been developed. A seemingly promising radiotracer,*N*-(6-[^{18}F]-fluorohexyl)-*N*-methylpropargylamine ([^{18}F]-FHMP) [81] was reported, but unfortunately a radioactive metabolite was detected in the rodent brain, mitigating against its use [82]. Two other potent and selective candidates for imaging brain MAO-B, namely, ^{11}C-radiolabeled 3-(4-[^{11}C]-methoxyphenyl)-6-methyl-2H-1-benzopyran-2-one and *N*-((1H-pyrrol-2-yl)methyl)-*N*-[^{11}C]-methyl-1-phenylmethanamine, were synthesized and evaluated in preclinical models [82]. While the distribution of the labeled benzopyranone did not match the regional MAO-B activity in rat brain, the labeled pyrrole had relatively high brain uptake, reflected regional MAO-B activity, and could be blocked, albeit with limited signal-to-background contrast. Two ^{11}C-labeled oxazolidinone derivatives have been reported as highly promising reversible MAO-B radiotracers: [^{11}C]-MD-230254 [83], and [^{11}C]-SL25.1188 (**Figure 5**) [84]. Both radiotracers entered brain, and obtained reversible specific binding to MAO-B in non-human primates, which could be blocked by L-deprenyl pre-treatment. High binding was present in the thalamus and striatum, and moderate binding in the cerebellum, which would preclude its use as a reference tissue. As with [^{11}C]-befloxatone, both of these compounds are obtained *via* the specialized labeling agent [^{11}C]-phosgene, such that their production has been restricted to only a few laboratories. [^{11}C]-SL25.1188 was efficiently labeled in one-step *via* [^{11}C]-CO_2 (**Figure 5**) at room temperature in solution, eliminating the use of [^{11}C]-$COCl_2$, and has been validated for human PET studies [85].

Acetylcholine esterase

Acetylcholine is a biogenic amine neurotransmitter synthesized in several populations of subcortical neurons, i.e. the large interneurons of the striatum, and the cortically-projecting neurons of the basal forebrain; degeneration of this latter population contributes to the cognitive impairment of AD. Developing a PET assay

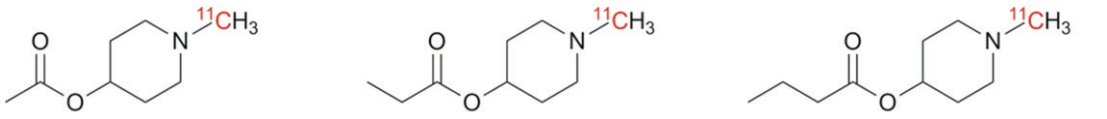

1-[^{11}C]methylpiperidin-4-yl acetate [^{11}C]-MP4A or [^{11}C]-AMP

1-[^{11}C]methylpiperidin-4-yl propionate [^{11}C]-PMP

1-[^{11}C]-methyl-4-piperidinyl *n*-butyrate [^{11}C]-MP4B or [^{11}C]-BMP

Figure 6. Structure of promising ^{11}C-radiolabeled acetylcholine esterase and butyrlcholine esterase ligands [88, 89].

for the synthesis of acetylcholine would be problematic due to the ubiquity of the precursors, acetate and choline. However, there are a number of PET methods for detecting acetylcholine esterase (AChE), the enzyme decomposing acetylcholine. Early imaging efforts focused on AChE inhibitor ligands, such as [^{11}C]-physostigmine [86], [^{11}C]-methyltacrine [86], and [^{11}C]-donezepil [87]. These inhibitor ligands have mostly been supplanted by a series of esters based on 1-[^{11}C]methylpiperidin-4-yl propionate ([^{11}C]-PMP) propionate (**Figure 6**) [88, 89]; here a labeled metabolite is formed in brain at a rate dependent upon the AChE activity, and is retained due to its considerable lipophilicity [89]. PET studies with [^{11}C]-PMP showed no change in AChE activity with normal aging [90], but revealed a 30-40% reduction in the temporal and parietal cortex of patients with AD [91]. The IC_{50} of the antidementia compound donezepil for blocking AChE has been estimated relative to observations of [^{11}C]-PMP uptake in monkey brain [92]; analogous studies in AD patients revealed a 30-40% blockade of AChE upon treatment with donezepil [93] or rivastigmine [94]. In a remarkable study in awake monkeys, treatment with donezepil increased acetylcholine levels in microdialysis samples from cortex, while decreasing [^{11}C]-PMP uptake, and likewise decreasing the binding in cerebral cortex of a PET ligand for muscarinic acetylcholine receptors [95], indicative of enhanced cholinergic signaling. However, persistent 30-40% blockade of [^{11}C]-PMP trapping did not influence the binding of [^{11}C]-nicotine at nicotinic receptors in cerebral cortex of AD patients treated with galantamine [96].

A study in early AD patients suggested that reductions in cortical and amygdala AChE activity precede measurable reductions in the basal forebrain, i.e. the location of the cholinergic neurons with ascending projections [97]. However, interpretation of results with AChE ligands is uncertain, since the cortical enzyme activity need not have a simple functional relationship with the integrity of the cortically-projecting cholinergic fibres. Furthermore, secretion of the "read through" variant of AChE to cerebral spinal fluid may be stimulated by galantamine treatment, without alterations in the synaptic variant; [^{11}C]-PMP PET cannot distinguish these forms of the enzyme [96]. Matters are made more complicated by the occurrence in brain of a distinct acetylcholine-hydrolyzing enzyme, butyrocholinesterase, which can be detected in PET studies with the more selective substrate 1-[^{11}C]-methyl-4-piperidinyl *n*-butyrate ([^{11}C]-MP4B) (**Figure 6**) [98]. Butyrocholinesterase activity may be increased in AD patients, especially those with the ApoE ε4 allele [99]; since acetylcholine is also a substrate for butyrocholinesterase, high levels of the latter enzyme may predict for poor response to selective AChE inhibitors.

Cytochrome P450/aromatase

Cytochrome (CYP) enzymes in liver and brain catalyze a variety of chemical reactions including demethylation and mono-oxidations of lipids, steroids and importantly exogenous toxins including drug molecules. CYP enzymes are implicated in ~75% of all metabolic transformations in drug toxicology [100] which can be associated with drug clearance, or activation. In the context of PET studies, CYP enzymes are relevant in that they mediate the catabolism of a number of radiotracers. For example, we have observed increased metabolism of [^{11}C]-deprenyl in patients with epilepsy [101], which we attribute to induction of liver enzymes by anticonvulsant medications; others have likewise noted increased metabolism of [^{11}C]-verapamil in epilepsy patients [102]. Bioavailability of the serotonin ligand [^{18}F]-FCWAY was increased in humans treated with the CYP2E1 inhibitor disulfuram [103]. Metabolism of the dopamine ligand raclopride may be attenuated by competition in pharmacological challenge studies with amphetamine [101, 104].

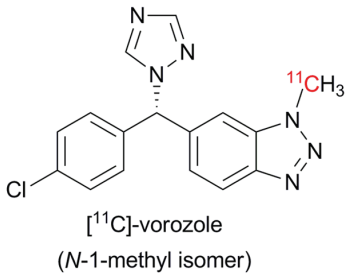

Figure 7. Structure of the aromatase inhibitor [^{11}C]-vorozole.

Recently, a cytochrome enzyme has emerged as an important target for brain PET. The product of the *CYP19A1* gene, known as aromatase, catalyzes the formation of estradiol from testosterone, and likewise the formation of estriol and estrone from other androgen precursors. Aromatase has a ubiquitous distribution throughout the body, and is expressed in a number of cell populations in brain, including pyramidal cells in the cerebral cortex, specific groups of neurons in the hippocampus, and cortical astrocytes [105]. Estrogen modulates neuroendocrine function and sexual dimorphism of the mammalian brain, and is also thought to influence synaptogenesis and neuronal survival. A number of transcripts of the single aromatase gene are differentially expressed in different brain regions [106]. The aromatase can now be visualized in brain with the inhibitor [^{11}C]-vorozole (**Figure 7**); it has highest autoradiographic binding in the medial amygdala, bed nucleus of stria terminalis, and preoptic area of male rat brain, with lesser expression in female rats [107]. Abundant displaceable binding of [^{11}C]-vorozole in the expected areas was detected in a PET study of young men, and also in a group of three women, for whom binding was higher in scans recorded at mid-cycle, when estrogen levels were highest, than during scans obtained in the menstrual/early follicular phase [108]. Intravenous administration of nicotine, at a dose comparable to that encountered in smoking, substantially blocked [^{11}C]-vorozole binding in brain of baboons [109]. This ligand promises to open up new domains of research in the neurobiology of addiction, ageing, gender differences in brain function, as well as in clinical oncology of estrogen-sensitive tumors.

Signal transduction inhibitors and second messengers

Phosphodiesterases

The G-protein coupled receptors (GPCRs) comprise a superfamily including most of the receptors of dopamine, serotonin and other biogenic amines, which exert their signaling though modulation of the intracellular levels of 3',5'-cyclic adenosine monophosphate (cAMP) and/or cyclic guanosine monophosphate (cGMP). The phosphodiester bonds in these compounds are hydrolyzed by phosphodiesterase (PDE) enzymes, which are classified into 11 families (PDE1 – PDE11), each of which has varying specificity for cAMP and cGMP. Further sub-categorization of these PDE enzyme families includes subfamilies of genes as well as splice variants derived from a single gene. The roles of PDEs as imaging targets in PET have been reviewed [110, 111].

The first reported attempt to target a PDE was conducted with the PDE4 antagonist ligand [^{11}C]-LY186126; although preliminary PET imaging revealed substantial binding in canine myocardium, this radiotracer was not further pursued [112]. A decade later, *ex vivo* biodistribution and pharmacological blocking studies were carried out in rats with [^{11}C]-Ro-20-1724 and [^{11}C]-(*R,S*)-rolipram [113]; the latter compound had good brain permeability, and bound in brain in a manner consistent with the known distribution of PDE4 enzyme. Subsequently, the enantiomer [^{11}C]-(*R*)-rolipram (**Figure 8**) was found to have to have higher binding in rat brain, and to have selectivity *in vivo* over PDE1 [114]. The first PDE4 imaging study in human brain soon followed [115].

PDE4 catalyzes the hydrolysis of cAMP, thereby terminating intracellular signaling through specific cAMP-dependent protein kinases. As such, activation of relevant receptors might be expected to deplete intracellular cAMP, which might in turn increase the availability of binding sites for PDE4 inhibitors. Based on this dynamic competition model, a number of pharmacological activation studies have been conducted with [^{11}C]-(*R*)-rolipram. For example, indirect agonism of catecholamine receptors increased PDE4 binding in brain of living monkeys *via* activation specifically of dopamine D1 receptors [95]. Activation of muscarinic receptors with scopolamine likewise increased PDE4 binding in that study. Attenuation of D1-mediated modulation of [^{11}C]-(*R*)-rolipram binding has been reported in aged monkey [116]. In a rat study *ex vivo*, MAO inhibition or treatment with selective noradrenalin or serotonin reuptake blockers

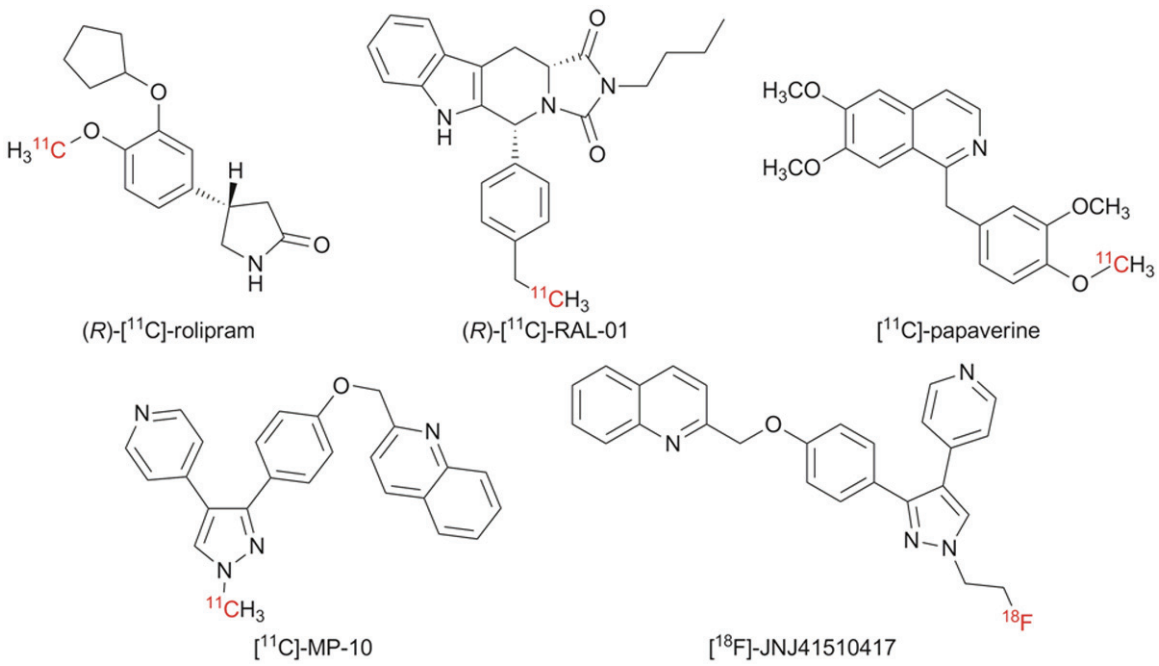

Figure 8. Structures of selected ^{11}C- and ^{18}F-radiolabeled PDE4, PDE5 and PDE10A inhibitors.

increased PDE4 binding, with roughly parallel changes in brain and myocardium [117]. Similar attenuation effects were observed in desipramine-challenged rats with diabetes evoked previously by a high fat diet [118]. However, others failed to detect increased PDE4 binding in brain of rats treated with imipramine [119]. These discrepant findings illustrate a limitation of second messenger studies; due to the convergence of multiple neurotransmitter signaling pathways, PET results with [^{11}C]-(*R*)-rolipram reflect the net modulation of the PDE4 enzyme. Thus, induction of anesthesia reduced the cerebral binding of [^{11}C]-(*R*)-rolipram [120], by an unknown mechanism presumably reflecting reduced tonic signaling by various biogenic amine neurotransmitters. Pharmacological activation of protein kinase A (PKA), which phosphorylates and activates PDE4, increased [^{11}C]-(*R*)-rolipram binding in rat brain, indicating an additional mechanism for convergence of intracellular signaling on PDE4 [121]. [^{11}C]-(*R*)-rolipram has advanced to studies in humans with major depressive disorder [122, 123].

Few other PDE imaging agents have been developed and evaluated in animal models. The cGMP-selective PDE5 has received considerable attention as the target of Sildenafil and related compounds. The distribution of the PDE5 inhibitor [^{11}C]-RAL-01 (**Figure 8**) was investigated in living pig [124]. This radiotracer readily entered the pig brain, and gave a hint of displaceable binding in the hypothalamus. In contrast, there was abundant displaceable binding in the myocardium, suggesting a potential application of [^{11}C]-RAL-01 in occupancy studies, especially given the use of PDE5 inhibitors for treating acute heart failure, and the linkage of myocardial PDE5 to adrenergic receptors.

PDE10A was identified independently by three groups in 1999 [125-127] and has a unique expression with mRNA levels in the brain [126]; the highest expression of PDE10A protein is in the medium spiny neurons of the striatum (caudate and putamen), nucleus accumbens, and olfactory tubercle [126-128]. PDE10A inhibitors are under development as novel approaches for treating neurological and psychiatric disorders such as schizophrenia, Parkinson's disease, and Huntington's disease [129, 130]. Testing of [^{11}C]-papaverine (**Figure 8**) and related derivatives revealed poor brain penetration and rapid washout from striatum in rats and monkeys [131]. Present work has focused on other candidate PDE10A radiotracers including *N*-alkylated pyrazoles labeled with ^{11}C, or ^{18}F such as [^{11}C]-MP-10 and [^{18}F]-JNJ41510417 (**Figure 8**) [132-136].

Adenylate cyclase

The intracellular activity of adenylate cyclase is stimulated directly with forskolin, a diterpene isolated from the rhizomes of *Coleus forskohlii,* which is a decorative garden plant. Activation of adenylate cyclase increases the intracellular levels of cAMP, which activates in turn protein kinase A (PKA). In the next step of the signalling cascade, PKA phosphorylates specific intracellular targets, including neuroreceptors. Activation of PKA also has consequences for energy metabolism, such that [^{18}F]-FDG PET can be used as a surrogate marker for activation of cAMP-dependent signal transduction in brain of living rats. These intriguing preclinical results suggest that forskolin binding changes could be relevant to addiction, epilepsy, and degenerative diseases. However, there have been few efforts to make corresponding PET ligands for adenylate cyclase. Many forskolin derivatives also bind to glucose transporters, including the GLUT1 residing in the blood-brain barrier, with affinity sometimes exceeding that for adenylate cyclase [137]. An ^{18}F-labeled forskolin derivative failed to enter brain of living rat [138], conceivably due to effects of P-glycoprotein (P-gp) at the blood-brain barrier. A study of the biodistribution of [^{11}C]-forskolin (**Figure 9**) indicated some entry into rat brain, but displaceable binding was only evident in myocardium [139], where adenylate cyclase mediates adrenergic signalling. This suggests that sympathetic denervation of the myocardium, as occurs frequently in Parkinson's disease, may present a natural model for investigating the effects of denervation on adenylate cyclase expression.

Protein kinases A, B and C

The intracellular concentration of cAMP is set by the balance of PDE and adenylate cyclase activities; a key mediator in the cellular response to cAMP is protein kinase A (PKA). Dysregulation of PKA in brain has been linked to depression and other affective disorders [140, 141]. In the only report of an attempt at molecular imaging of PKA, carbon-11 labeled *N*-(2-(4-bromocinnamylamino)-ethyl)-*N*-methyl-isoquinoline-5-sulfonamide, an *N*-methyl derivative of the known PKA inhibitor H89 (**Figure 10**), proved to have inadequate brain penetration [142].

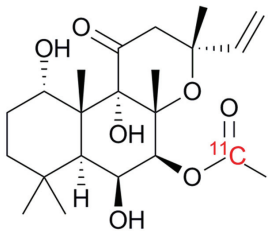

[^{11}C]-forskolin

Figure 9. Structure of the adenylate cyclase binding radiotracer [^{11}C]-forskolin.

While PKB (also known as Akt) is more frequently investigated in the context of oncology, it is also implicated in brain signalling pathways, via interactions with PI3K and glycogen synthase kinase-3 β (GSK-3β). Recently, a [^{11}C]-bisaryl-maleimide was proposed for imaging PKB but has yet to be evaluated *in vivo* (**Figure 10**) [143]. Several attempts have also been made to develop radiotracers for imaging PKC, the Ca^{2+}/calmodulin-dependent protein kinase. PKC is also part of the PI3K signaling pathway, and therefore, plays a crucial role in intracellular signal transduction. Carbon-11 labeled phorbol esters have been used for PET imaging of PKC in brain [144]. Other efforts to develop PET tracers for PKC focused on labeling a staurosporine derivative with ^{11}C [145].

As PKC enzymes are activated by signals such as increases of Ca^{2+} or diacylglycerol (DAG), other work has investigated [^{11}C]-DAGs but these radiotracers were found to metabolize in rat brain to phosphatidylinositols and phosphatidylinositol phosphates [146]. The trapping in brain was partially indicative of phosphotidylinositol turnover, and could be stimulated by cholinergic mechanisms [144, 147].

Glycogen synthase kinase-3β

The glycogen synthase activity is under the regulation of glycogen synthase kinase-3β which is a serine/threonine kinase. This enzyme is highly abundant in brain tissues and is involved in signal transduction cascades controlling multiple cellular processes. Small molecule inhibitors of GSK-3β are currently under development as potential medications for diverse neurological illnesses including depression, stroke, and bipolar disorder [148], and recently a "GSK-3 hypothesis of Alzheimer's disease" has been proposed [149]. One potent and selective inhibitor of GSK-3β, namely *N*-(4-methoxy)-*N*'-(5-nitro-1,3-thiazole-2-yl)urea, has

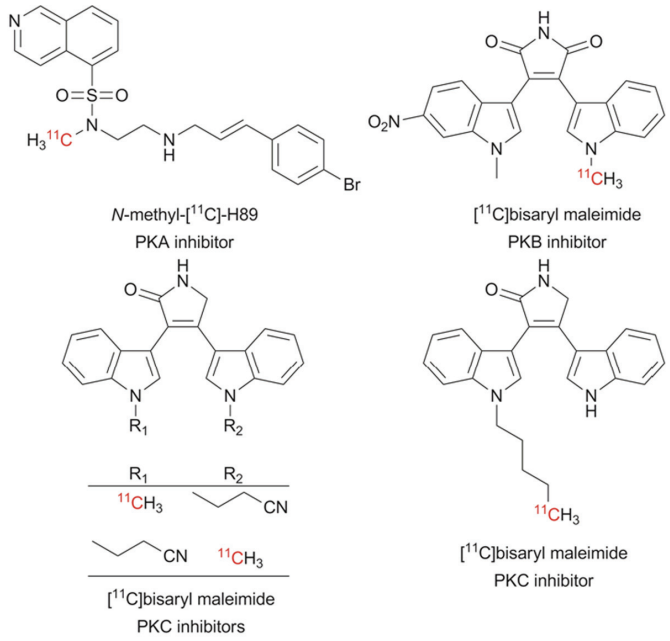

Figure 10. Structures of selected ^{11}C-radiolabeled protein kinase A, B and C inhibitors [142].

been successfully labeled with ^{11}C (**Figure 11**), but, *ex vivo* biodistribution studies showed very low uptake of in brain of conscious rodents, despite pre-administration of a P-glycoprotein inhibitor [150]. More recently, [^{11}C]CO_2 fixation was used to prepare [^{11}C-carbonyl]-AR-A014418 (**Figure 11**), thereby enabling libraries of related radiolabeled derivatives to be prepared based on this scaffold [151]. Future work focusing on systematic generation of derivatives of related inhibitors promises to yield useful radiopharmaceuticals for imaging GSK-3β.

Arachidonic acid (AA)

Arachidonic acid is derived from phospholipids by the action of phospholipase A2, or from diacylglycerol by the action of a lipase. In addition to serving as a precursor for inflammatory eicosanoids and anandamide, arachidonic acid in the nervous system is involved in signalling cascades regulating ion channels and PKC. In preclinical testing of 20-[^{18}F]-fluoroarachidonic acid there was considerable uptake in myocardium, but little evidence of labeling of brain lipids [152, 153]. Myocardial fatty acid uptake is presumably more indicative of energy metabolism than intracellular signalling. Subsequently, [^{11}C]-arachidonic acid was tested by PET in monkeys. The net influx was unaffected by a three-fold increase in CBF under conditions of hypocapnea, indicating that it is driven by a trapping process in brain, rather than simply delivery. In a PET study of healthy, young awake humans, in which [^{11}C]-arachidonic acid net uptake was corrected for the formation in brain of [^{11}C]-CO_2, there was no discernible decline in the magnitude for [^{11}C]-arachidonic acid uptake with healthy aging [154]. Brain uptake of [^{11}C]-arachidonic acid was globally *increased* in grey matter of patients with AD [155]. This finding was especially evident in neocortical regions known to have a high burden of amyloid plaques, which suggested that the tracer uptake reveals an inflammatory process mediated by microglia.

Pre-treatment of rats with the non-selective dopamine agonist apomorphine increased [^{11}C]-arachidonic acid influx in the basal ganglia and various cortical regions [156]. This stimulation was blocked by raclopride pre-treatment, indicating that it was mediated by D_2 receptor activation. A low dose of the more selective dopamine D_2 agonist quinpirole stimulated [^{11}C]-arachidonic acid uptake in the striatum of awake rats, whereas as higher dose also had effects in cerebral cortex; pre-treatment with lithium attenuated the D_2-receptor mediated stimulation of tracer uptake [157], suggesting a basis for the efficacy of lithium in bipolar disorder. Stimulation with a flashing light increased [^{11}C]-arachidonic acid uptake in visual cortex and other cortical regions of healthy humans, in a pattern generally overlapping with stimulus-evoked increases in CBF [158]. However, there have been no [^{11}C]-arachidonic acid PET studies of human seizure disorders, or for that matter, affective disorders. Despite certain preclinical findings implicating fatty acids in dopamine transmission, the cerebral uptake of [^{11}C]-arachidonic acid has yet to be investigated in patients with Parkinson's disease.

Fatty acid amide hydrolase (FAAH)

There has been a recent surge of reports on the preparation of PET radiotracers targeting fatty acid amide hydrolase (FAAH), the enzyme responsible for metabolising the endogenous

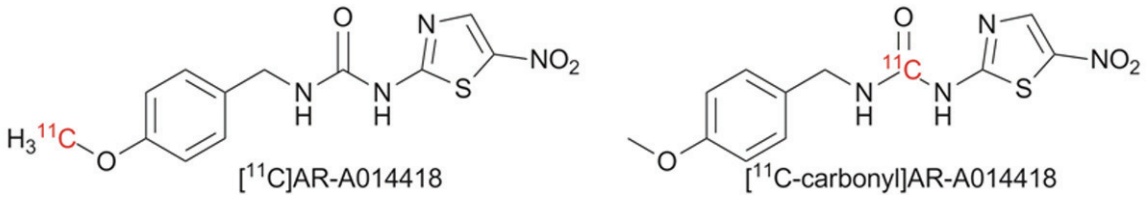

Figure 11. Structures of two ^{11}C-radiolabeled isotopologues of the GSK-3β inhibitor AR-A014418 [150, 151].

cannabinoid anandamide. The earliest reports investigated [^{11}C]-labeled analogues of URB597, which exhibited low brain uptake and rapid metabolism [159]. In a preliminary report, radiosynthesis and PET imaging studies of a reversible FAAH inhibitor, [^{11}C]-MK-3168 (**Figure 12**) in non-human primates and healthy volunteers under baseline and blocking conditions was conducted [160]. An analogue of URB597, [^{11}C]-CURB (**Figure 12**) is an irreversible carbamate inhibitor of FAAH with similar selectivity but greater brain penetration than URB597. To avoid the potential loss of the radiolabel during hydrolysis by FAAH, [^{11}C]-CURB was radiolabeled at the carbonyl position involved in the carbamylation of Ser241, such that the label remains bound to the enzyme [161]. Evaluation of [^{11}C]-CURB in rodents demonstrated high brain uptake with distribution matching that of FAAH expression, and displayed irreversible binding kinetics which could be blocked by intraperitoneal pretreatment with high doses URB597 or URB694 [161]. This radiotracer is currently undergoing preliminary investigation in healthy human volunteers and showed greater uptake in FAAH rich regions including the cerebral cortex, cerebellum, and hippocampus with lowest uptake in the hypothalamus [162]. Several other derivatives are under investigation [163]. Optimization of a urea-based lead compound led to the synthesis of PF-04457845 as a potent and highly selective FAAH inhibitor [164] which underwent Phase II clinical trials for managing pain [165] as well as for marijuana withdrawal. Based on this structure, Skaddan *et al.* [166] recently reported the preparation of [^{18}F]-PF-9811 (**Figure 12**), in which the trifluoromethyl group of PF-04457845 was substituted by a [^{18}F]-fluoroethyl group. Although they reported minimal loss of FAAH inhibitor potency or selectivity *in vitro*, the uptake and specific binding in rodent brain was modest. A preliminary report of the radiosynthesis of [^{11}C]-PF-04457845 (**Figure 12**) and its *ex vivo* biodistribution in conscious rodent models shows promise for imaging FAAH [167].

Prostanoid biosynthesis

The biosynthesis of the prostanoid is mediated by the enzyme arachidonic acid cyclo-oxygenase, which comes in two common variants known as COX-1 and COX-2. Whereas COX-1 is a constituent of normal cells, COX-2 expression is inducible, being most abundant in reactive macrophages. A number of ^{11}C-labeled arylpropionic acids and their methyl esters, including [^{11}C]-ibuprofen [168] and [^{11}C]-ketoprofen-methyl ester [169] have been prepared as potential PET tracers for COX-1 (**Figure 13**) [170]. Inflammatory expression of COX-1 in mouse brain could be revealed with [^{11}C]-ketoprofen-methyl ester [171]; transient increases in binding *ex vivo* were evoked by intracerebral injections of lipopolysaccharide or quinolinic acid, in association with increased activated microglia and macrophages at the site of inflammation. Considerable efforts have been expended towards development of COX-2 tracers, for application in molecular imaging studies of oncology and also neurodegenerative disease. Some specific binding of the COX-2 ligand [^{11}C]-rofecoxib (**Figure 13**) was evident in normal rat brain, but induction of encephalitis via Herpes Simplex infection did not evoke the expected increase in specific binding [172]. The COX-2 ligand [^{11}C]-celecoxib has been prepared, but its fitness for detecting inflammatory responses is not yet established and the radiotracer is known to undergo metabolism giving [^{11}C]-SC-62807 which is rapidly cleared *via* hepatobiliary excretion [173]. However, displaceable uptake of an ^{18}F-labeled derivative of celecoxib (**Figure 13**) was evident in solid tumor xenografts in nude mice [174].

Conclusions

There are relatively few brain enzymatic processes of sufficient abundance such that their activity can be measured by molecular imaging of product formation *in vivo*. Whereas the great

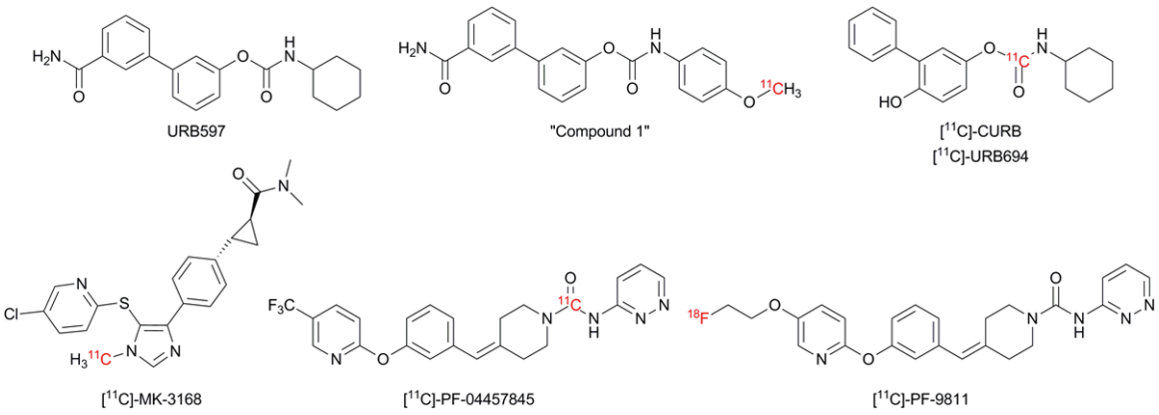

Figure 12. Structures of selected ^{11}C- and ^{18}F-radiolabeled FAAH inhibitors.

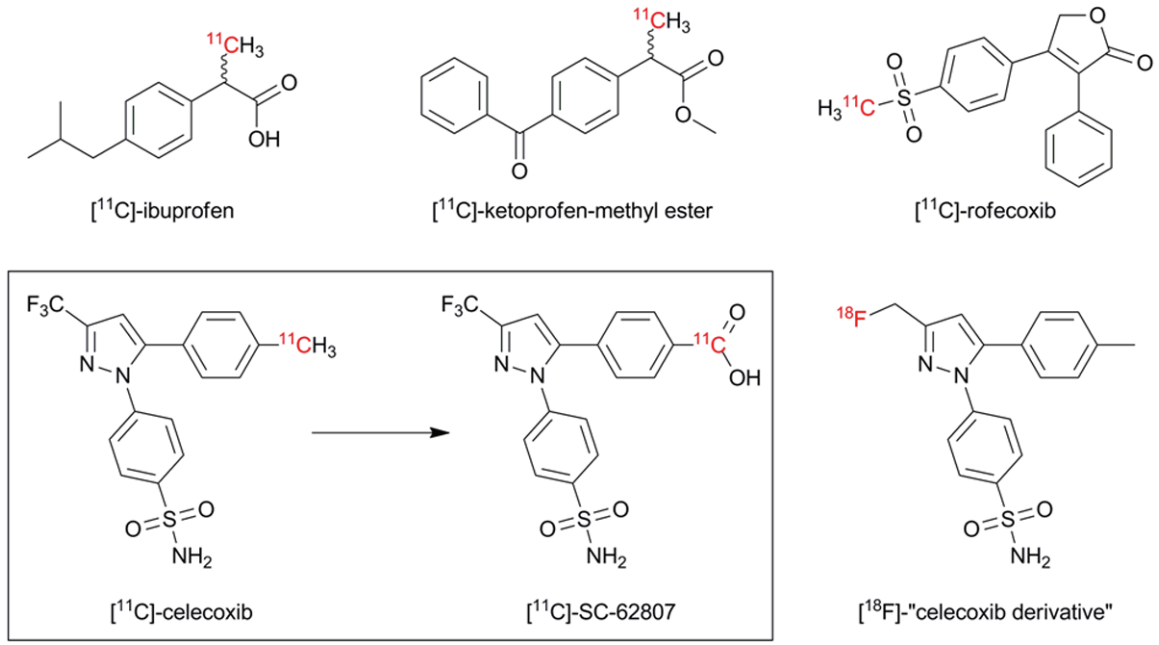

Figure 13. Structures of selected ^{11}C- and ^{18}F-radiolabeled COX inhibitors.

majority of useful brain tracers are reversible ligands for neuroreceptors and transporters, the signal transduction pathways linked to neuroreceptors present a wide range of targets which have scarcely been investigated by molecular imaging. Efforts to pursue new target classes, as well as to explore more diverse radiochemical scaffolds, offers great potential for improving the specificity of brain imaging.

Acknowledgments

We thank Dr. Torsten Kuwert for fruitful discussions and helpful comments. JPH gratefully acknowledges financial support from the Australian Nuclear Science and Technology Organisation (ANSTO).

Address correspondence to: Dr. Neil Vasdev, Division of Nuclear Medicine and Molecular Imaging, Massachusetts General Hospital, and Department of Radiology, Harvard Medical School, 55 Fruit St., White 427, Boston, MA 02114, USA. Phone: +1-617-643-4736; Fax: +1-617-726-6165; E-mail: vasdev.neil@mgh.harvard.edu

References

[1] Cumming P and Vasdev N. Molecular imaging studies of second messenger pathways: Looking deeper than the membrane. In: Gründer G,

editors. Molecular Imaging in the Clinical Neurosciences. Humana Press; 2012. pp: 137-148.
[2] Cumming P and Vasdev N. The assay of enzyme activity by positron emission tomography. In: Gründer G, editors. Molecular Imaging in the Clinical Neurosciences. Humana Press; 2012. pp: 111-135.
[3] Phelps ME, Huang SC, Hoffman EJ, Selin C, Sokoloff L and Kuhl DE. Tomographic measurement of local cerebral glucose metabolic rate in humans with (F-18)2-fluoro-2-deoxy-D-glucose: Validation of method. Ann Neurol 1979; 6: 371-388.
[4] Maher F, Vannucci SJ and Simpson IA. Glucose transporter proteins in brain. FASEB J 1994; 8: 1003-1011.
[5] Bohnen NI, Djang DSW, Herholz K, Anzai Y and Minoshima S. Effectiveness and Safety of ^{18}F-FDG PET in the evaluation of dementia: A review of the recent literature. J Nucl Med 2012; 53: 59-71.
[6] Mosconi L, Mistur R, Switalski R, Tsui WH, Glodzik L, Li Y, Pirraglia E, De Santi S, Reisberg B, Wisniewski T and de Leon MJ. FDG-PET changes in brain glucose metabolism from normal cognition to pathologically verified Alzheimer's disease. Eur J Nucl Med Mol Imaging 2009; 36: 811-822.
[7] Alavi A, Yakir S and Newberg AB. Positron emission tomography in seizure disorders. Ann New York Acad Sci 2011; 1228: E1-E12.
[8] Comar D, Cartron J, Maziere M and Marazano C. Labelling and metabolism of methionine-methyl-^{11}C. Eur J Nucl Med 1976; 1: 11-14.
[9] Christensen HN. Role of amino acid transport and countertransport in nutrition and metabolism. Physiol Rev 1990; 70: 43-77.
[10] Bustany P, Chatel M, Derlon JM, Darcel F, Sgouropoulos P, Soussaline F and Syrota A. Brain tumor protein synthesis and histological grades: a study by positron emission tomography (PET) with C11-L-Methionine. J Neurooncol 1986; 3: 397-404.
[11] Singhal T, Narayanan TK, Jain V, Mukherjee J and Mantil J. ^{11}C-L-methionine positron emission tomography in the clinical management of cerebral gliomas. Mol Imaging Biol 2008; 10: 1-18.
[12] Lindner KJ, Hartvig P, Akesson C, Tyrefors N, Sundin A and Langstrom B. Analysis of L-[methyl-^{11}C]methionine and metabolites in human plasma by an automated solid-phase extraction and a high-performance liquid chromatographic procedure. J Chromatogr B Biomed Appl 1996; 679: 13-19.
[13] Ishiwata K, Vaalburg W, Elsinga PH, Paans AM and Woldring MG. Comparison of L-[1-^{11}C] methionine and L-methyl-[^{11}C]methionine for measuring in vivo protein synthesis rates with PET. J Nucl Med 1988; 29: 1419-1427.
[14] Ishiwata K, Vaalburg W, Elsinga PH, Paans AM and Woldring MG. Metabolic studies with L-[1-^{14}C]tyrosine for the investigation of a kinetic model to measure protein synthesis rates with PET. J Nucl Med 1988; 29: 524-529.
[15] Salmon E, Gregoire MC, Delfiore G, Lemaire C, Degueldre C, Franck G and Comar D. Combined study of cerebral glucose metabolism and [^{11}C]methionine accumulation in probable Alzheimer's disease using positron emission tomography. J Cereb Blood Flow Metab 1996; 16: 399-408.
[16] Hoeksma M, Reijngoud DJ, Pruim J, de Valk HW, Paans AM and van Spronsen FJ. Phenylketonuria: High plasma phenylalanine decreases cerebral protein synthesis. Mol Genet Metab 2009; 96: 177-182.
[17] Bishu S, Schmidt KC, Burlin TV, Channing MA, Horowitz L, Huang T, Liu ZH, Qin M, Vuong BK, Unterman AJ, Xia Z, Zametkin A, Herscovitch P, Quezado Z and Smith CB. Propofol anesthesia does not alter regional rates of cerebral protein synthesis measured with L-[1-(11)C]leucine and PET in healthy male subjects. J Cereb Blood Flow Metab 2009; 29: 1035-1047.
[18] Qin M, Schmidt KC, Zametkin AJ, Bishu S, Horowitz LM, Burlin TV, Xia Z, Huang T, Quezado ZM and Smith CB. Altered cerebral protein synthesis in fragile X syndrome: studies in human subjects and knockout mice. J Cereb Blood Flow Metab 2013; Epub ahead of print.
[19] Chishty M, Begley DJ, Abbott JN and Reichel A. Functional characterisation of nucleoside transport in rat brain endothelial cells. Neuroreport 2003; 14: 1087-1090.
[20] Shields AF, Lim K, Grierson J, Link J and Krohn KA. Utilization of labeled thymidine in DNA synthesis: studies for PET. J Nucl Med 1990; 31: 337-342.
[21] Shields AF, Grierson JR, Dohmen BM, Machulla HJ, Stayanoff JC, Lawhorn-Crews JM, Obradovich JE, Muzik O and Mangner TJ. Imaging proliferation in vivo with [F-18]FLT and positron emission tomography. Nat Med 1998; 4: 1334-1336.
[22] Chen W, Delaloye S, Silverman DH, Geist C, Czernin J, Sayre J, Satyamurthy N, Pope W, Lai A, Phelps ME and Cloughesy T. Predicting treatment response of malignant gliomas to bevacizumab and irinotecan by imaging proliferation with [^{18}F] fluorothymidine positron emission tomography: a pilot study. J Clin Oncol 2007; 25: 4714-4721.
[23] Ullrich R, Backes H, Li H, Kracht L, Miletic H, Kesper K, Neumaier B, Heiss WD, Wienhard K and Jacobs AH. Glioma proliferation as assessed by 3'-fluoro-3'-deoxy-L-thymidine positron

emission tomography in patients with newly diagnosed high-grade glioma. Clin Cancer Res 2008; 14: 2049-2055.

[24] Garnett ES, Firnau G and Nahmias C. Dopamine visualized in the basal ganglia of living man. Nature 1983; 305: 137-138.

[25] Garnett S, Firnau G, Nahmias C and Chirakal R. Striatal dopamine metabolism in living monkeys examined by positron emission tomography. Brain Res 1983; 280: 169-171.

[26] Leenders KL, Poewe WH, Palmer AJ, Brenton DP and Frackowiak RS. Inhibition of L-[^{18}F]fluorodopa uptake into human brain by amino acids demonstrated by positron emission tomography. Ann Neurol 1986; 20: 258-262.

[27] Cumming P, Hausser M, Martin WR, Grierson J, Adam MJ, Ruth TJ and McGeer EG. Kinetics of in vitro decarboxylation and the in vivo metabolism of 2-^{18}F- and 6-^{18}F-fluorodopa in the hooded rat. Biochem Pharmacol 1988; 37: 247-250.

[28] Endres CJ, Swaminathan S, DeJesus OT, Sievert M, Ruoho AE, Murali D, Rommelfanger SG and Holden JE. Affinities of dopamine analogs for monoamine granular and plasma membrane transporters: implications for PET dopamine studies. Life Sci 1997; 60: 2399-2406.

[29] Kumakura Y and Cumming P. PET studies of cerebral levodopa metabolism: a review of clinical findings and modeling approaches. Neuroscientist 2009; 15: 635-650.

[30] Creveling CR and Kirk KL. The effect of ring-fluorination on the rate of O-methylation of dihydroxyphenylalanine (DOPA) by catechol-O-methyltransferase: significance in the development of ^{18}F-PET scanning agents. Biochem Biophys Res Commun 1985; 130: 1123-1131.

[31] Boyes BE, Cumming P, Martin WR and McGeer EG. Determination of plasma [^{18}F]-6-fluorodopa during positron emission tomography: elimination and metabolism in carbidopa treated subjects. Life Sci 1986; 39: 2243-2252.

[32] Cumming P, Boyes BE, Martin WR, Adam M, Ruth TJ and McGeer EG. Altered metabolism of [^{18}F]-6-fluorodopa in the hooded rat following inhibition of catechol-O-methyltransferase with U-0521. Biochem Pharmacol 1987; 36: 2527-2531.

[33] Dhawan V, Ishikawa T, Patlak C, Chaly T, Robeson W, Belakhlef A, Margouleff C, Mandel F and Eidelberg D. Combined FDOPA and 3OMFD PET studies in Parkinson's disease. J Nucl Med 1996; 37: 209-216.

[34] Cumming P, Boyes BE, Martin WR, Adam M, Grierson J, Ruth T and McGeer EG. The metabolism of [^{18}F]6-fluoro-L-3,4-dihydroxyphenylalanine in the hooded rat. J Neurochem 1987; 48: 601-608.

[35] Huang SC, Yu DC, Barrio JR, Grafton S, Melega WP, Hoffman JM, Satyamurthy N, Mazziotta JC and Phelps ME. Kinetics and modeling of L-6-[^{18}F]fluoro-dopa in human positron emission tomographic studies. J Cereb Blood Flow Metab 1991; 11: 898-913.

[36] Kumakura Y, Danielsen EH, Gjedde A, Vernaleken I, Buchholz HG, Heinz A, Grunder G, Bartenstein P and Cumming P. Elevated [(18)F] FDOPA utilization in the periaqueductal gray and medial nucleus accumbens of patients with early Parkinson's disease. Neuroimage 2010; 49: 2933-2939.

[37] Sawle GV, Wroe SJ, Lees AJ, Brooks DJ and Frackowiak RS. The identification of presymptomatic parkinsonism: clinical and [^{18}F]dopa positron emission tomography studies in an Irish kindred. Ann Neurol 1992; 32: 609-617.

[38] Morrish PK, Rakshi JS, Bailey DL, Sawle GV and Brooks DJ. Measuring the rate of progression and estimating the preclinical period of Parkinson's disease with [^{18}F]dopa PET. J Neurol Neurosurg Psych 1998; 64: 314-319.

[39] Rakshi JS, Pavese N, Uema T, Ito K, Morrish PK, Bailey DL and Brooks DJ. A comparison of the progression of early Parkinson's disease in patients started on ropinirole or L-dopa: an ^{18}F-dopa PET study. J Neural Transm 2002; 109: 1433-1443.

[40] Reith J, Benkelfat C, Sherwin A, Yasuhara Y, Kuwabara H, Andermann F, Bachneff S, Cumming P, Diksic M, Dyve SE, Etienne P, Evans AC, Lal S, Shevell M, Savard G, Wong DF, Chouinard G and Gjedde A. Elevated dopa decarboxylase activity in living brain of patients with psychosis. Proc Natl Acad Sci 1994; 91: 11651-11654.

[41] Kumakura Y, Cumming P, Vernaleken I, Buchholz HG, Siessmeier T, Heinz A, Kienast T, Bartenstein P and Grunder G. Elevated [^{18}F]fluorodopamine turnover in brain of patients with schizophrenia: an [^{18}F]fluorodopa/positron emission tomography study. J Neurosci 2007; 27: 8080-8087.

[42] Hagberg GE, Torstenson R, Marteinsdottir I, Fredrikson M, Langstrom B and Blomqvist G. Kinetic compartment modeling of [^{11}C]-5-hydroxy-L-tryptophan for positron emission tomography assessment of serotonin synthesis in human brain. J Cereb Blood Flow Metab 2002; 22: 1352-1366.

[43] Shoaf SE, Carson RE, Hommer D, Williams WA, Higley JD, Schmall B, Herscovitch P, Eckelman WC and Linnoila M. The suitability of [^{11}C]-alpha-methyl-L-tryptophan as a tracer for serotonin synthesis: studies with dual administration of [^{11}C] and [^{14}C] labeled tracer. J Cereb Blood Flow Metab 2000; 20: 244-252.

[44] Leyton M, Diksic M and Benkelfat C. Brain regional alpha-[^{11}C]methyl-L-tryptophan trapping correlates with post-mortem tissue serotonin content and [^{11}C]5-hydroxytryptophan accumulation. Int J Neuropsychopharmacol 2005; 8: 633-634.

[45] Rosa-Neto P, Diksic M, Okazawa H, Leyton M, Ghadirian N, Mzengeza S, Nakai A, Debonnel G, Blier P and Benkelfat C. Measurement of brain regional alpha-[^{11}C]methyl-L-tryptophan trapping as a measure of serotonin synthesis in medication-free patients with major depression. Arch Gen Psych 2004; 61: 556-563.

[46] Leyton M, Paquette V, Gravel P, Rosa-Neto P, Weston F, Diksic M and Benkelfat C. alpha-[^{11}C]Methyl-L-tryptophan trapping in the orbital and ventral medial prefrontal cortex of suicide attempters. Eur Neuropsychopharmacol 2006; 16: 220-223.

[47] Berney A, Nishikawa M, Benkelfat C, Debonnel G, Gobbi G and Diksic M. An index of 5-HT synthesis changes during early antidepressant treatment: alpha-[^{11}C]methyl-L-tryptophan PET study. Neurochem Int 2008; 52: 701-708.

[48] Juhasz C, Chugani DC, Muzik O, Shah A, Asano E, Mangner TJ, Chakraborty PK, Sood S and Chugani HT. Alpha-methyl-L-tryptophan PET detects epileptogenic cortex in children with intractable epilepsy. Neurology 2003; 60: 960-968.

[49] Fedi M, Reutens DC, Andermann F, Okazawa H, Boling W, White C, Dubeau F, Nakai A, Gross DW, Andermann E and Diksic M. alpha-[^{11}C]-Methyl-L-tryptophan PET identifies the epileptogenic tuber and correlates with interictal spike frequency. Epilepsy Res 2003; 52: 203-213.

[50] Kitahama K, Maeda T, Denney RM and Jouvet M. Monoamine oxidase: distribution in the cat brain studied by enzyme- and immunohistochemistry: recent progress. Prog Neurobiol 1994; 42: 53-78.

[51] Nakamura S and Vincent SR. Histochemistry of MPTP oxidation in the rat brain: sites of synthesis of the parkinsonism-inducing toxin MPP+. Neurosci Lett 1986; 65: 321-325.

[52] Fowler JS, Logan J, Volkow ND, Wang GJ, MacGregor RR and Ding YS. Monoamine oxidase: radiotracer development and human studies. Methods 2002; 27: 263-277.

[53] Fowler JS, Logan J, Volkow ND and Wang GJ. Translational neuroimaging: positron emission tomography studies of monoamine xidase. Mol Imaging Biol 2005; 7: 377-387.

[54] Moerlein SM, Stocklin G, Pawlik G, Wienhard K and Heiss WD. Regional cerebral pharmacokinetics of the dopaminergic neurotoxin 1-methyl-4-phenyl-1,2,3,6-tetrahydropyridine as examined by positron emission tomography in a baboon is altered by tranylcypromine. Neurosci Lett 1986; 66: 205-209.

[55] Hartvig P, Larsson BS, Lindberg BS, Oreland L, Gullberg P, Langstrom B, Rimland A, Lundqvist H, Malmborg P and Lindquist NG. Influence of monoamine oxidase inhibitors and a dopamine uptake blocker on the distribution of ^{11}C-N-methyl-4-phenyl-1,2,3,6-tetrahydropyridine, ^{11}C-MPTP, in the head of the rhesus monkey. Acta Neurol Scand 1986; 74: 10-16.

[56] Fowler JS, MacGregor RR, Wolf AP, Arnett CD, Dewey SL, Schlyer D, Christman D, Logan J, Smith M, Sachs H, et al. Mapping human brain monoamine oxidase A and B with ^{11}C-labeled suicide inactivators and PET. Science 1987; 235: 481-485.

[57] Fowler JS, Wolf AP, MacGregor RR, Dewey SL, Logan J, Schlyer DJ and Langstrom B. Mechanistic positron emission tomography studies: demonstration of a deuterium isotope effect in the monoamine oxidase-catalyzed binding of [^{11}C]L-deprenyl in living baboon brain. J Neurochem 1988; 51: 1524-1534.

[58] Kumlien E, Nilsson A, Hagberg G, Langstrom B and Bergstrom M. PET with ^{11}C-deuterium-deprenyl and ^{18}F-FDG in focal epilepsy. Acta Neurol Scand 2001; 103: 360-366.

[59] Hirvonen J, Kailajarvi M, Haltia T, Koskimies S, Nagren K, Virsu P, Oikonen V, Sipila H, Ruokoniemi P, Virtanen K, Scheinin M and Rinne JO. Assessment of MAO-B occupancy in the brain with PET and [^{11}C]-L-deprenyl-D2: a dose-finding study with a novel MAO-B inhibitor, EVT 301. Clin Pharmacol Ther 2009; 85: 506-512.

[60] Fowler JS, Volkow ND, Wang GJ, Pappas N, Logan J, MacGregor R, Alexoff D, Wolf AP, Warner D, Cilento R and Zezulkova I. Neuropharmacological actions of cigarette smoke: brain monoamine oxidase B (MAO B) inhibition. J Addict Dis 1998; 17: 23-34.

[61] Fowler JS, Wang GJ, Volkow ND, Franceschi D, Logan J, Pappas N, Shea C, MacGregor RR and Garza V. Smoking a single cigarette does not produce a measurable reduction in brain MAO B in non-smokers. Nicotine Tob Res 1999; 1: 325-329.

[62] Fowler JS, Logan J, Ding YS, Franceschi D, Wang GJ, Volkow ND, Pappas N, Schlyer D, Gatley SJ, Alexoff D, Felder C, Biegon A and Zhu W. Non-MAO A binding of clorgyline in white matter in human brain. J Neurochem 2001; 79: 1039-1046.

[63] Fowler JS, Volkow ND, Wang GJ, Pappas N, Logan J, Shea C, Alexoff D, MacGregor RR, Schlyer DJ, Zezulkova I and Wolf AP. Brain monoamine oxidase A inhibition in cigarette smokers. Proc Natl Acad Sci 1996; 93: 14065-14069.

[64] Jensen SB, Di Santo R, Olsen AK, Pedersen K, Costi R, Cirilli R and Cumming P. Synthesis and

cerebral uptake of 1-(1-[^{11}C]Methyl-1H-pyrrol-2-yl)-2-phenyl-2-(1-pyrrolidinyl)ethanone, a novel tracer for positron emission tomography studies of monoamine oxidase type A. J Med Chem 2008; 51: 1617-1622.

[65] Bergstrom M, Westerberg G, Nemeth G, Traut M, Gross G, Greger G, Muller-Peltzer H, Safer A, Eckernas SA, Grahner A and Langstrom B. MAO-A inhibition in brain after dosing with esuprone, moclobemide and placebo in healthy volunteers: in vivo studies with positron emission tomography. Eur J Clin Pharmacol 1997; 52: 121-128.

[66] Sacher J, Houle S, Parkes J, Rusjan PM, Sagrati S, Wilson AA and Meyer JH. Monoamine oxidase A inhibitor occupancy during treatment of major depressive episodes with moclobemide and St. John's wort: A [^{11}C] harmine PET study. Biol Psychiatry 2010; 67: 146S-147S.

[67] Leroy C, Bragulat V, Berlin I, Gregoire MC, Bottlaender M, Roumenov D, Dolle F, Bourgeois S, Penttila J, Artiges E, Martinot JL and Trichard C. Cerebral monoamine oxidase A inhibition in tobacco smokers confirmed with PET and [^{11}C]befloxatone. J Clin Psychopharmacol 2009; 29: 86-88.

[68] Dolle F, Valette H, Bramoulle Y, Guenther I, Fuseau C, Coulon C, Lartizien C, Jegham S, George P, Curet O, Pinquier JL and Bottlaender M. Synthesis and in vivo imaging properties of [^{11}C]befloxatone: A novel highly potent positron emission tomography ligand for mono-amine oxidase-A. Bioorg Med Chem Lett 2003; 13: 1771-1775.

[69] Bacher I, Houle S, Xu X, Zawertailo L, Soliman A, Wilson AA, Selby P, George TP, Sacher J, Miler L, Kish SJ, Rusjan P, Meyer JH. Monoamine oxidase a binding in the prefrontal and anterior cingulate cortices during acute withdrawal from heavy cigarette smoking. Arch Gen Psych 2011; 68: 817-826.

[70] Pedersen K, Simonsen M, Ostergaard SD, Munk OL, Rosa-Neto P, Olsen AK, Jensen SB, Moller A and Cumming P. Mapping the amphetamine-evoked changes in [^{11}C]raclopride binding in living rat using small animal PET: modulation by MAO-inhibition. Neuroimage 2007; 35: 38-46.

[71] Jensen SB, Olsen AK, Pedersen K and Cumming P. Effect of monoamine oxidase inhibition on amphetamine-evoked changes in dopamine receptor availability in the living pig: a dual tracer PET study with [^{11}C]harmine and [^{11}C] raclopride. Synapse 2006; 59: 427-434.

[72] Meyer JH, Ginovart N, Boovariwala A, Sagrati S, Hussey D, Garcia A, Young T, Praschak-Rieder N, Wilson AA and Houle S. Elevated monoamine oxidase a levels in the brain: an explanation for the monoamine imbalance of major depression. Arch Gen Psych 2006; 63: 1209-1216.

[73] Meyer JH, Wilson AA, Sagrati S, Miler L, Rusjan P, Bloomfield PM, Clark M, Sacher J, Voineskos AN and Houle S. Brain monoamine oxidase A binding in major depressive disorder: relationship to selective serotonin reuptake inhibitor treatment, recovery, and recurrence. Arch Gen Psych 2009; 66: 1304-1312.

[74] Sacher J, Wilson AA, Houle S, Rusjan P, Hassan S, Bloomfield PM, Stewart DE and Meyer JH. Elevated brain monoamine oxidase A binding in the early postpartum period. Arch Gen Psych 2010; 67: 468-474.

[75] Sacher J, Rabiner EA, Clark M, Rusjan P, Soliman A, Boskovic R, Kish SJ, Wilson AA, Houle S and Meyer JH. Dynamic, adaptive changes in MAO-A binding after alterations in substrate availability: an in vivo [^{11}C]-harmine positron emission tomography study. J Cereb Blood Flow Metab 2012; 32: 443-446.

[76] Macwhorter SE and Baldwin RM. Synthesis and biodistribution of ^{123}I N-(2-aminoethyl)-5-iodo-2-pyridinecarboxamide (Ro 43-0463), a monoamine oxidase B inhibitor. Int J Rad Appl Instrum B 1991; 18: 563-564.

[77] Blauenstein P, Remy N, Buck A, Ametamey S, Haberli M and Schubiger PA. In vivo properties of *N*-(2-aminoethyl)-5-halogeno-2-pyridinecarboxamide ^{18}F- and ^{123}I-labelled reversible inhibitors of monoamine oxidase B. Nucl Med Biol 1998; 25: 47-52.

[78] Plenevaux A, Dewey SL, Fowler JS, Guillaume M and Wolf AP. Synthesis of (*R*)-(-)- and (*S*)-(+)-4-fluorodeprenyl and (*R*)-(-)- and (*S*)-(+)-[*N*-^{11}C-*methyl*]-4-fluorodeprenyl and positron emission tomography studies in baboon brain. J Med Chem 1990; 33: 2015-2019.

[79] Plenevaux A, Fowler JS, Dewey SL, Wolf AP and Guillaume M. The Synthesis of No-carrier-added DL-4-[^{18}F]Fluorodeprenyl via the Nucleophilic Aromatic Substitution Reaction. Appl Radiat Isot 1991; 42: 121-127.

[80] Nag S, Lehmann L, Kettschau G, Heinrich T, Thiele A, Varrone A, Gulyas B and Halldin C. Synthesis and evaluation of [^{18}F]fluororasagiline, a novel positron emission tomography (PET) radioligand for monoamine oxidase B (MAO-B). Bioorg Med Chem 2012; 20: 3065-3071.

[81] Mukherjee J, Yang ZY and Lew R. N-(6-^{18}F-Fluorohexyl)-N-Methylpropargylamine: A fluorine-18-labeled monoamine oxidase B inhibitor for potential use in PET studies. Nucl Med Biol 1999; 26: 111-116.

[82] Vasdev N, Sadovski O, Moran MD, Parkes J, Meyer JH, Houle S and Wilson AA. Development of new radiopharmaceuticals for imaging

monoamine oxidase B. Nucl Med Biol 2011; 38: 933-943.

[83] Bernard S, Fuseau C, Schmid L, Milcent R and Crouzel C. Synthesis and in vivo studies of a specific monoamine oxidase B inhibitor: 5-[4-(benzyloxy)phenyl]-3-(2-cyanoethyl)-1,3,4-oxadiazol-[^{11}C]-2(3*H*)-one. Eur J Nucl Med 1996; 23: 150-156.

[84] Saba W, Valette H, Peyronneau MA, Bramoulle Y, Coulon C, Curet O, George P, Dolle F and Bottlaender M. [(11)C]SL25.1188, a new reversible radioligand to study the monoamine oxidase type B with PET: preclinical characterisation in nonhuman primate. Synapse 2010; 64: 61-69.

[85] Vasdev N, Sadovski O, Garcia A, Dollé F, Meyer JH, Houle S and Wilson AA. Radiosynthesis of [^{11}C]SL25.1188 via [^{11}C]CO_2 fixation for imaging monoamine oxidase B. J Labelled Compds Radiopharm 2011; 54: 678-680.

[86] Tavitian B, Pappata S, Planas AM, Jobert A, Bonnot-Lours S, Crouzel C and DiGiamberardino L. In vivo visualization of acetylcholinesterase with positron emission tomography. Neuroreport 1993; 4: 535-538.

[87] De Vos F, Santens P, Vermeirsch H, Dewolf I, Dumont F, Slegers G, Dierckx RA and De Reuck J. Pharmacological evaluation of [^{11}C]donepezil as a tracer for visualization of acetylcholinesterase by PET. Nucl Med Biol 2000; 27: 745-747.

[88] Snyder SE, Tluczek L, Jewett DM, Nguyen TB, Kuhl DE and Kilbourn MR. Synthesis of 1-[^{11}C] methylpiperidin-4-yl propionate ([^{11}C]PMP) for in vivo measurements of acetylcholinesterase activity. Nucl Med Biol 1998; 25: 751-754.

[89] Kilbourn MR, Snyder SE, Sherman PS and Kuhl DE. In vivo studies of acetylcholinesterase activity using a labeled substrate, N-[^{11}C]methylpiperdin-4-yl propionate ([^{11}C]PMP). Synapse 1996; 22: 123-131.

[90] Kuhl DE, Koeppe RA, Minoshima S, Snyder SE, Ficaro EP, Foster NL, Frey KA and Kilbourn MR. In vivo mapping of cerebral acetylcholinesterase activity in aging and Alzheimer's disease. Neurology 1999; 52: 691-699.

[91] Iyo M, Namba H, Fukushi K, Shinotoh H, Nagatsuka S, Suhara T, Sudo Y, Suzuki K and Irie T. Measurement of acetylcholinesterase by positron emission tomography in the brains of healthy controls and patients with Alzheimer's disease. Lancet 1997; 349: 1805-1809.

[92] Shiraishi T, Kikuchi T, Fukushi K, Shinotoh H, Nagatsuka S, Tanaka N, Ota T, Sato K, Hirano S, Tanada S, Iyo M and Irie T. Estimation of plasma IC50 of donepezil hydrochloride for brain acetylcholinesterase inhibition in monkey using N-[^{11}C]methylpiperidin-4-yl acetate ([^{11}C]MP4A) and PET. Neuropsychopharmacol 2005; 30: 2154-2161.

[93] Ota T, Shinotoh H, Fukushi K, Kikuchi T, Sato K, Tanaka N, Shimada H, Hirano S, Miyoshi M, Arai H, Suhara T and Irie T. Estimation of plasma IC50 of donepezil for cerebral acetylcholinesterase inhibition in patients with Alzheimer disease using positron emission tomography. Clin Neuropharmacol 2010; 33: 74-78.

[94] Kaasinen V, Nagren K, Jarvenpaa T, Roivainen A, Yu M, Oikonen V, Kurki T and Rinne JO. Regional effects of donepezil and rivastigmine on cortical acetylcholinesterase activity in Alzheimer's disease. J Clin Psychopharmacol 2002; 22: 615-620.

[95] Tsukada H, Nishiyama S, Fukumoto D, Ohba H, Sato K and Kakiuchi T. Effects of acute acetylcholinesterase inhibition on the cerebral cholinergic neuronal system and cognitive function: Functional imaging of the conscious monkey brain using animal PET in combination with microdialysis. Synapse 2004; 52: 1-10.

[96] Kadir A, Darreh-Shori T, Almkvist O, Wall A, Grut M, Strandberg B, Ringheim A, Eriksson B, Blomquist G, Langstrom B and Nordberg A. PET imaging of the in vivo brain acetylcholinesterase activity and nicotine binding in galantamine-treated patients with AD. Neurobiol Aging 2008; 29: 1204-1217.

[97] Herholz K, Weisenbach S, Zundorf G, Lenz O, Schroder H, Bauer B, Kalbe E and Heiss WD. In vivo study of acetylcholine esterase in basal forebrain, amygdala, and cortex in mild to moderate Alzheimer disease. Neuroimage 2004; 21: 136-143.

[98] Roivainen A, Rinne J, Virta J, Jarvenpaa T, Salomaki S, Yu M and Nagren K. Biodistribution and blood metabolism of 1-^{11}C-methyl-4-piperidinyl n-butyrate in humans: an imaging agent for in vivo assessment of butyrylcholinesterase activity with PET. J Nucl Med 2004; 45: 2032-2039.

[99] Darreh-Shori T, Forsberg A, Modiri N, Andreasen N, Blennow K, Kamil C, Ahmed H, Almkvist O, Langstrom B and Nordberg A. Differential levels of apolipoprotein E and butyrylcholinesterase show strong association with pathological signs of Alzheimer's disease in the brain in vivo. Neurobiol Aging 2011; 32: e15-e32.

[100] Guengerich FP. Cytochrome P450 and chemical toxicology. Chem Res Toxicol 2007; 21: 70-83.

[101] Cumming P, Yokoi F, Chen A, Deep P, Dagher A, Reutens D, Kapczinski F, Wong DF and Gjedde A. Pharmacokinetics of radiotracers in human plasma during positron emission tomography. Synapse 1999; 34: 124-134.

[102] Abrahim A, Luurtsema G, Bauer M, Karch R, Lubberink M, Pataraia E, Joukhadar C, Kletter

K, Lammertsma A, Baumgartner C, Müller M and Langer O. Peripheral metabolism of (*R*)-[^{11}C]verapamil in epilepsy patients. Eur J Nucl Med Mol Imaging 2008; 35: 116-123.

[103] Ryu YH, Liow JS, Zoghbi S, Fujita M, Collins J, Tipre D, Sangare J, Hong J, Pike VW and Innis RB. Disulfiram Inhibits Defluorination of ^{18}F-FCWAY, Reduces Bone Radioactivity, and Enhances Visualization of Radioligand Binding to Serotonin 5-HT1A Receptors in Human Brain. J Nucl Med 2007; 48: 1154-1161.

[104] Østergaard SD, Alstrup AKO, Gramsbergen JB, Minuzzi L, Pedersen K, Jensen SB, Doudet D and Cumming P. MDMA-evoked changes in the binding of dopamine D2 receptor ligands in striatum of rats with unilateral serotonin depletion. Synapse 2010; 64: 70-82.

[105] Azcoitia I, Yague JG and Garcia-Segura LM. Estradiol Synthesis Within The Human Brain. Neuroscience 2011; 191: 139-47.

[106] Sasano H, Takashashi K, Satoh F, Nagura H and Harada N. Aromatase in the human central nervous system. Clin Endocrinol 1998; 48: 325-329.

[107] Takahashi K, Bergstrom M, Frandberg P, Vesstrom EL, Watanabe Y and Langstrom B. Imaging of aromatase distribution in rat and rhesus monkey brains with [^{11}C]vorozole. Nucl Med Biol 2006; 33: 599-605.

[108] Biegon A, Kim SW, Alexoff DL, Jayne M, Carter P, Hubbard B, King P, Logan J, Muench L, Pareto D, Schlyer D, Shea C, Telang F, Wang GJ, Xu Y and Fowler JS. Unique distribution of aromatase in the human brain: in vivo studies with PET and [*N*-methyl-^{11}C]vorozole. Synapse 2010; 64: 801-807.

[109] Biegon A, Kim SW, Logan J, Hooker JM, Muench L and Fowler JS. Nicotine blocks brain estrogen synthase (aromatase): in vivo positron emission tomography studies in female baboons. Biol Psychiatry 2010; 67: 774-777.

[110] Andrés JI, De Angelis M, Alcázar J, Celen S and Bormans G. Recent advances in positron emission tomography (PET) radiotracers for imaging phosphodiesterases. Curr Top Med Chem 2012; 12: 1224-1236.

[111] Kenk M, Thomas A, Lortie M, Dekemp R, Beanlands RS and Dasilva JN. PET measurements of cAMP-mediated phosphodiesterase-4 with (R)-[^{11}C]rolipram. Curr Radiopharm 2011; 4: 44-58.

[112] Prenant C, Crouzel C, Valois JM, Robertson DW and Comar D. Synthesis of [11C]LY186126, an inhibitor of phosphodiesterase. Appl Radiat Isot 1992; 43: 946-948.

[113] Lourenco CM, DaSilva JN, Warsh JJ, Wilson AA and Houle S. Imaging of cAMP-specific phosphodiesterase-IV: comparison of [^{11}C]rolipram and [^{11}C]Ro 20-1724 in rats. Synapse 1999; 31: 41-50.

[114] Lourenco CM, Houle S, Wilson AA and DaSilva JN. Characterization of R-[^{11}C]rolipram for PET imaging of phosphodiesterase-4: in vivo binding, metabolism, and dosimetry studies in rats. Nucl Med Biol 2001; 28: 347-358.

[115] DaSilva J, Lourenco C, Meyer J, Hussey D, Potter W and Houle S. Imaging cAMP-specific phosphodiesterase-4 in human brain with R-[^{11}C]rolipram and positron emission tomography. Eur J Nucl Med Mol Imaging 2002; 29: 1680-1683.

[116] Harada N, Nishiyama S, Ohba H, Sato K, Kakiuchi T and Tsukada H. Age differences in phosphodiesterase type-IV and its functional response to dopamine D1 receptor modulation in the living brain: a PET study in conscious monkeys. Synapse 2002; 44: 139-145.

[117] Lourenco CM, Kenk M, Beanlands RS and DaSilva JN. Increasing synaptic noradrenaline, serotonin and histamine enhances in vivo binding of phosphodiesterase-4 inhibitor (R)-[^{11}C] rolipram in rat brain, lung and heart. Life Sci 2006; 79: 356-364.

[118] Greene M, Thackeray JT, Kenk M, Thorn SL, Bevilacqua L, Harper ME, Beanlands RS and DaSilva JN. Reduced in vivo phosphodiesterase-4 response to acute noradrenaline challenge in diet-induced obese rats. Can J Physiol Pharm 2009; 87: 196-202.

[119] Fujita M, Imaizumi M, D'Sa C, Zoghbi SS, Crescenzo MS, Hong J, Musachio JL, Gee AD, Seidel J, Green MV, Pike VW, Duman RS and Innis RB. In vivo and in vitro measurement of brain phosphodiesterase 4 in rats after antidepressant administration. Synapse 2007; 61: 78-86.

[120] Itoh T, Abe K, Zoghbi SS, Inoue O, Hong J, Imaizumi M, Pike VW, Innis RB and Fujita M. PET Measurement of the In Vivo Affinity of ^{11}C-(R)-Rolipram and the Density of Its Target, Phosphodiesterase-4, in the Brains of Conscious and Anesthetized Rats. J Nucl Med 2009; 50: 749-756.

[121] Itoh T, Abe K, Hong J, Inoue O, Pike VW, Innis RB and Fujita M. Effects of cAMP-dependent protein kinase activator and inhibitor on in vivo rolipram binding to phosphodiesterase 4 in conscious rats. Synapse 2010; 64: 172-176.

[122] Zanotti-Fregonara P, Hines CS, Zoghbi SS, Liow JS, Zhang Y, Pike VW, Drevets WC, Mallinger AG, Zarate CA Jr, Fujita M and Innis RB. Population-based input function and image-derived input function for [^{11}C](R)-rolipram PET imaging: Methodology, validation and application to the study of major depressive disorder. Neuroimage 2012; 63: 1532-1541.

[123] Fujita M, Hines CS, Zoghbi SS, Mallinger AG, Dickstein LP, Liow JS, Zhang Y, Pike VW, Drevets WC, Innis RB and Zarate CA. Downregulation of brain phosphodiesterase type IV measured with ^{11}C-(R)-Rolipram positron emission tomography in major depressive disorder. Biol Psych 2012; 72: 548-554.

[124] Jakobsen S, Kodahl GM, Olsen AK and Cumming P. Synthesis, radiolabeling and in vivo evaluation of [^{11}C]RAL-01, a potential phosphodiesterase 5 radioligand. Nucl Med Biol 2006; 33: 593-597.

[125] Loughney K, Snyder PB, Uher L, Rosman GJ, Ferguson K and Florio VA. Isolation and characterization of PDE10A, a novel human 3′, 5′-cyclic nucleotide phosphodiesterase. Gene 1999; 234: 109-117.

[126] Soderling SH, Bayuga SJ and Beavo JA. Isolation and characterization of a dual-substrate phosphodiesterase gene family: PDE10A. Proc Natl Acad Sci 1999; 96: 7071-7076.

[127] Fujishige K, Kotera J, Michibata H, Yuasa K, Takebayashi SI, Okumura K and Omori K. Cloning and characterization of a novel human phosphodiesterase that hydrolyzes both cAMP and cGMP (PDE10A). J Biol Chem 1999; 274: 18438-18445.

[128] Coskran TM, Morton D, Menniti FS, Adamowicz WO, Kleiman RJ, Ryan AM, Strick CA, Schmidt CJ and Stephenson DT. Immunohistochemical localization of phosphodiesterase 10A in multiple mammalian species. J Histochem Cytochem 2006; 54: 1205-1213.

[129] Menniti FS, Faraci WS and Schmidt CJ. Phosphodiesterases in the CNS: targets for drug development. Nat Rev Drug Discov 2006; 5: 660-670.

[130] Hebb ALO, Robertson HA and Denovan-Wright EM. Striatal phosphodiesterase mRNA and protein levels are reduced in Huntington′s disease transgenic mice prior to the onset of motor symptoms. Neuroscience 2004; 123: 967-981.

[131] Tu Z, Xu J, Jones LA, Li S and Mach RH. Carbon-11 labeled papaverine as a PET tracer for imaging PDE10A: radiosynthesis, in vitro and in vivo evaluation. Nucl Med Biol 2010; 37: 509-516.

[132] Plisson C, Salinas C, Weinzimmer D, Labaree D, Lin SF, Ding YS, Jakobsen S, Smith PW, Eiji K, Carson RE, Gunn RN and Rabiner EA. Radiosynthesis and in vivo evaluation of [^{11}C]MP-10 as a positron emission tomography radioligand for phosphodiesterase 10A. Nucl Med Biol 2011; 38: 875-884.

[133] Celen S, Koole M, De Angelis M, Sannen I, Chitneni SK, Alcazar J, Dedeurwaerdere S, Moechars D, Schmidt M, Verbruggen A, Langlois X, Van Laere K, Andrés JI and Bormans G. Preclinical Evaluation of ^{18}F-JNJ41510417 as a Radioligand for PET Imaging of Phosphodiesterase-10A in the Brain. J Nucl Med 2010; 51: 1584-1591.

[134] Tu Z, Fan J, Li S, Jones LA, Cui J, Padakanti PK, Xu J, Zeng D, Shoghi KI, Perlmutter JS and Mach RH. Radiosynthesis and in vivo evaluation of [^{11}C]MP-10 as a PET probe for imaging PDE10A in rodent and non-human primate brain. Bioorg Med Chem 2011; 19: 1666-1673.

[135] Laere K, Ahmad R, Hudyana H, Celen S, Dubois K, Schmidt M, Bormans G and Koole M. Human biodistribution and dosimetry of ^{18}F-JNJ42259152, a radioligand for phosphodiesterase 10A imaging. Eur J Nucl Med Mol Imaging 2013; 40: 254-261.

[136] Andrés JI, De Angelis M, Alcázar Js, Iturrino L, Langlois X, Dedeurwaerdere S, Lenaerts I, Vanhoof G, Celen S and Bormans G. Synthesis, In Vivo Occupancy, and Radiolabeling of Potent Phosphodiesterase Subtype-10 Inhibitors as Candidates for Positron Emission Tomography Imaging. J Med Chem 2011; 54: 5820-5835.

[137] Appel NM, Robbins JD, De Souza EB and Seamon KB. [^{125}I]-labeled forskolin analogs which discriminate adenylyl cyclase and a glucose transporter: pharmacological characterization and localization of binding sites in rat brain by in vitro receptor autoradiography. J Pharmacol Exper Therapeutics 1992; 263: 1415-1423.

[138] Kiesewetter DO, Sassaman MB, Robbins J, Jagoda EM, Carson RE, Appel NM, Sutkowski E, Herscovitch P, Braun A and Eckelman WC. Synthesis and evaluation of an ^{18}F analog of forskolin for imaging adenylyl cyclase. J Fluorine Chem 2000; 101: 297-304.

[139] Sasaki T, Enta A, Nozaki T, Ishii SI and Senda M. Carbon-11-Forskolin: A ligand for visualization of the adenylate cyclase-related second messenger system. J Nucl Med 1993; 34: 1944-1948.

[140] Taylor SS, Kim C, Vigil D, Haste NM, Yang J, Wu J and Anand GS. Dynamics of signaling by PKA. Biochim Biophys Acta 2005; 1754: 25-37.

[141] Duman Rs, Heninger GR, Nestler EJ. A molecular and cellular theory of depression. Arch Gen Psych 1997; 54: 597-606.

[142] Vasdev N, LaRonde FJ, Woodgett JR, Garcia A, Rubie EA, Meyer JH, Houle S and Wilson AA. Rationally designed PKA inhibitors for positron emission tomography: Synthesis and cerebral biodistribution of N-(2-(4-bromocinnamylamino)ethyl)-N-[^{11}C]methyl-isoquinoline-5-sulfonamide. Bioorg Med Chem 2008; 16: 5277-5284.

[143] Wang M, Gao M, Miller KD, Sledge GW, Hutchins GD and Zheng QH. The first design and synthesis of [^{11}C]MKC-1 ([^{11}C]Ro 31-7453), a new

potential PET cancer imaging agent. Nucl Med Biol 2010; 37: 763-775.
[144] Ohmori Y, Imahori Y, Ueda S, Fujii R, Ido T, Wakita K and Nakahashi H. Protein kinase C imaging using carbon-11-labeled phorbol esters: 12-Deoxyphorbol 13-isobutyrate-20-[1-^{11}C]butyrate as the potential ligand for positron emission tomography. J Nucl Med 1993; 34: 431-439.
[145] Sasaki T, Ishii SI, Senda M, Akinaga S and Murakata C. Synthesis of [7ß-methoxy ^{11}C] methoxy staurosporine for imaging protein kinase C localization in the brain. Appl Radiat Isot 1996; 47: 67-69.
[146] Imahori Y, Fujii R, Ueda S, Matsumoto K, Wakita K, Ido T, Nariai T and Nakahashi H. Membrane Trapping of Carbon-11-Labeled 1,2-Diacylglycerols as a Basic Concept for Assessing Phosphatidylinositol Turnover in Neurotransmission Process. J Nucl Med 1992; 33: 413-422.
[147] Imahori Y, Fujii R, Ueda S, Ohmori Y, Wakita K and Matsumoto K. Phosphoinositide turnover imaging linked to muscarinic cholinergic receptor in the central nervous system by positron emission tomography. J Nucl Med 1993; 34: 1543-1551.
[148] Martinez A, Castro A, Medina M and Wang B. Glycogen synthase kinase 3 (GSK-3) and its inhibitors: Drug discovery and development. Hoboken, New York: John Wiley & Sons Inc. 2006.
[149] Hernández F and Avila J. The role of glycogen synthase kinase 3 in the early stages of Alzheimers' disease. FEBS Letters 2008; 582: 3848-3854.
[150] Vasdev N, Garcia A, Stableford WT, Young AB, Meyer JH, Houle S and Wilson AA. Synthesis and ex vivo evaluation of carbon-11 labelled N-(4-methoxybenzyl)-N′-(5-nitro-1,3-thiazol-2-yl)urea ([11C]AR-A014418): A radiolabelled glycogen synthase kinase-3β specific inhibitor for PET studies. Bioorg Med Chem Lett 2005; 15: 5270-5273.
[151] Hicks JW, Wilson AA, Rubie EA, Woodgett JR, Houle S and Vasdev N. Towards the preparation of radiolabeled 1-aryl-3-benzyl ureas: Radiosynthesis of [^{11}C-carbonyl] AR-A014418 by [^{11}C]CO2 fixation. Bioorg Med Chem Lett 2012; 22: 2099-2101.
[152] Nagatsugi F, Hokazono J, Sasaki S and Maeda M. Synthesis of 20-[^{18}F]fluoroarachidonic acid: A potential phospholipid metabolic agent. J Labelled Compds Radiopharm 1994; 34: 1121-1127.
[153] Pichika R, Taha AY, Gao F, Kotta K, Cheon Y, Chang L, Kiesewetter D, Rapoport SI and Eckelman WC. The synthesis and in vivo pharmacokinetics of fluorinated arachidonic acid: Implications for imaging neuroinflammation. J Nucl Med 2012; 53: 1383-1391.
[154] Giovacchini G, Lerner A, Toczek MT, Fraser C, Ma K, DeMar JC, Herscovitch P, Eckelman WC, Rapoport SI and Carson RE. Brain Incorporation of ^{11}C-Arachidonic Acid, Blood Volume, and Blood Flow in Healthy Aging: A Study With Partial-Volume Correction. J Nucl Med 2004; 45: 1471-1479.
[155] Esposito G, Giovacchini G, Liow JS, Bhattacharjee AK, Greenstein D, Schapiro M, Hallett M, Herscovitch P, Eckelman WC, Carson RE and Rapoport SI. Imaging neuroinflammation in Alzheimer's disease with radiolabeled arachidonic acid and PET. J Nucl Med 2008; 49: 1414-1421.
[156] Bhattacharjee A, Chang L, White L, Bazinet R and Rapoport S. Imaging apomorphine stimulation of brain arachidonic acid signaling via D2-like receptors in unanesthetized rats. Psychopharmacol 2008; 197: 557-566.
[157] Basselin M, Chang L, Bell JM and Rapoport SI. Chronic lithium chloride administration to unanesthetized rats attenuates brain dopamine D2-like receptor-initiated signaling via arachidonic acid. Neuropsychopharmacol 2005; 30: 1064-1075.
[158] Esposito G, Giovacchini G, Der M, Liow JS, Bhattacharjee AK, Ma K, Herscovitch P, Channing M, Eckelman WC, Hallett M, Carson RE and Rapoport SI. Imaging signal transduction via arachidonic acid in the human brain during visual stimulation, by means of positron emission tomography. Neuroimage 2007; 34: 1342-1351.
[159] Wyffels L, Muccioli GG, Kapanda CN, Labar G, De Bruyne S, De Vos F and Lambert DM. PET imaging of fatty acid amide hydrolase in the brain: synthesis and biological evaluation of an ^{11}C-labelled URB597 analogue. Nucl Med Biol 2010; 37: 665-675.
[160] Joshi A, Li W, Sanabria S, Holahan M, Purcell M, Declercq R, Depre M, Bormans G, Van Laere K and Hamill T. Translational studies with [^{11}C]MK-3168, a PET tracer for fatty acid amide hydrolase (FAAH). J Nucl Med 2012; 53 Suppl 1: 121P.
[161] Wilson AA, Garcia A, Parkes J, Houle S, Tong J and Vasdev N. [^{11}C]CURB: Evaluation of a novel radiotracer for imaging fatty acid amide hydrolase by positron emission tomography. Nucl Med Biol 2011; 38: 247-253.
[162] Rusjan PM, Wilson AA, Mizrahi R, Boileau I, Chavez SE, Lobaugh NJ, Kish SJ, Houle S and Tong J. Mapping human brain fatty acid amide hydrolase activity with PET. J Cereb Blood Flow Metab 2012; 33: 407-14.
[163] Wilson AA, Hicks JW, Sadovski O, Parkes J, Tong J, Houle S, Fowler CJ and Vasdev N. Ra-

diosynthesis and evaluation of [^{11}C-carbonyl]-labeled carbamates as fatty acid amide hydrolase radiotracers for positron emission tomography. J Med Chem 2013; 56: 201-209.

[164] Johnson DS, Stiff C, Lazerwith SE, Kesten SR, Fay LK, Morris M, Beidler D, Liimatta MB, Smith SE, Dudley DT, Sadagopan N, Bhattachar SN, Kesten SJ, Nomanbhoy TK, Cravatt BF and Ahn K. Discovery of PF-04457845: A highly potent, orally bioavailable, and selectiveurea FAAH inhibitor. Med Chem Lett 2011; 2: 91-96.

[165] Huggins JP, Smart TS, Langman S, Taylor L and Young T. An efficient randomised, placebo-controlled clinical trial with the irreversible fatty acid amide hydrolase-1 inhibitor PF-04457845, which modulates endocannabinoids but fails to induce effective analgesia in patients with pain due to osteoarthritis of the knee. Pain 2012; 153: 1837-1846.

[166] Skaddan MB, Zhang L, Johnson DS, Zhu A, Zasadny KR, Coelho RV, Kuszpit K, Currier G, Fan KH, Beck EM, Chen L, Drozda SE, Balan G, Niphakis M, Cravatt BF, Ahn K, Bocan T and Villalobos A. The synthesis and in vivo evaluation of [^{18}F]PF-9811: a novel PET ligand for imaging brain fatty acid amide hydrolase (FAAH). Nucl Med Biol 2012; 39: 1058-1067.

[167] Hicks JW, Sadovski O, Parkes J, Fowler CJ, Houle S, Tong J, Vasdev N and Wilson AA. Evaluation of a small library of carbamates and ureas, including PF-04457845, as potential imaging agents for fatty acid amide hydrolase (FAAH). J Cereb Blood Flow Metab 2012; 32: S17.

[168] Kikuchi T, Okada M, Nengaki N, Furutsuka K, Wakizaka H, Okamura T, Zhang MR and Kato K. Efficient synthesis and chiral separation of ^{11}C-labeled ibuprofen assisted by DMSO for imaging of *in vivo* behavior of the individual isomers by positron emission tomography. Bioorg Med Chem 2011; 19: 3265-3273.

[169] Shukuri M, Takashima-Hirano M, Tokuda K, Matsumura K, Goto M, Doi H, Suzuki M, Watanabe Y and Onoe H. A novel PET probe, ^{11}C-ketoprofen-methyl ester, targeting cyclooxygenase-1 in the brain. J Nucl Med 2011; 52 Suppl 1: 224.

[170] Takashima-Hirano M, Shukuri M, Takashima T, Goto M, Wada Y, Watanabe Y, Onoe H, Doi H and Suzuki M. General method for the ^{11}C-labeling of 2-arylpropionic acids and their esters: Construction of a PET tracer library for a study of biological events involved in COXs expression. Chem Eur J 2010; 16: 4250-4258.

[171] Shukuri M, Takashima-Hirano M, Tokuda K, Takashima T, Matsumura K, Inoue O, Doi H, Suzuki M, Watanabe Y and Onoe H. In vivo expression of cyclooxygenase-1 in activated microglia and macrophages during neuroinflammation visualized by PET with ^{11}C-ketoprofen methyl ester. J Nucl Med 2011; 52: 1094-1101.

[172] de Vries EF, Doorduin J, Dierckx RA and van Waarde A. Evaluation of [^{11}C]rofecoxib as PET tracer for cyclooxygenase 2 overexpression in rat models of inflammation. Nucl Med Biol 2008; 35: 35-42.

[173] Takashima-Hirano M, Takashima T, Katayama Y, Wada Y, Sugiyama Y, Watanabe Y, Doi H and Suzuki M. Efficient sequential synthesis of PET Probes of the COX-2 inhibitor [^{11}C]celecoxib and its major metabolite [^{11}C]SC-62807 and *in vivo* PET evaluation. Bioorg Med Chem 2011; 19: 2997-3004.

[174] Uddin MJ, Crews BC, Ghebreselasie K, Huda I, Kingsley PJ, Ansari MS, Tantawy MN, Reese J and Marnett LJ. Fluorinated COX-2 inhibitors as agents in PET imaging of inflammation and cancer. Cancer Prevention Res 2011; 4: 1536-1545.

[175] Sundin A, Eriksson B, BergstrÖM M, LÅNgstrÖM B, ÖBerg K and ÖRlefors H. PET in the diagnosis of neuroendocrine tumors. Ann New York Acad Sci 2004; 1014: 246-257.

[176] Dolle F, Bramoulle Y, Hinnen F and Fowler JS. Efficient synthesis and formulation of (R)-(−)-[^{11}C]Deprenyl, a selective radioligand for the quantification of MAO-B activity using PET. J Labelled Compds Radiopharm 2002; 45: 803-811.

[177] Fowler JS, Logan J, Wang GJ, Volkow ND, Telang F, Ding YS, Shea C, Garza V, Xu Y, Li Z, Alexoff D, Vaska P, Ferrieri R, Schlyer D, Zhu W and John Gatley S. Comparison of the binding of the irreversible monoamine oxidase tracers, [^{11}C]clorgyline and [^{11}C]l-deprenyl in brain and peripheral organs in humans. Nucl Med Biol 2004; 31: 313-319.

[178] Bergström M, Westerberg G and Långström B. ^{11}C-harmine as a tracer for monoamine oxidase a (MAO-A): In vitro and in vivo studies. Nucl Med Biol 1997; 24: 287-293.